

A nanovaccine for immune activation and prophylactic protection of atherosclerosis in mouse models

Received: 8 October 2023

Accepted: 24 February 2025

Published online: 02 March 2025



Lei Zhang^{1,9}, Abdulrahman AL-Ammari^{2,9}, Danxuan Zhu³, Hongsong Zhang^{1,4}, Peng Zhou¹, Xu Zhi⁵, Weixiao Ding¹, Xinmeng Li¹, Qingqing Yu¹, Yuwen Gai¹, Xiaoling Ma³, Chuntao Chen¹, Chao Zuo⁶, Jiaan Zhang⁷, Wanying Zhu⁸ & Dongping Sun¹✉

Vaccines offer prophylactic treatments against atherosclerosis by eliciting effector T cell and antibody responses, which require effective delivery of antigen and adjuvant to activate dendritic cells (DC). Here we show that individual conjugation of antigen p210 and adjuvant CpG oligodeoxynucleotides onto superparamagnetic iron oxide nanoparticles formulates a nanovaccine cocktail that activates DCs for antigen cross-presentation and induction of co-stimulatory signals, cytokines and CD8⁺ effector/effector memory T cell responses. This nanovaccine modulates the DCs in the draining lymph nodes, activates both CD4⁺ and CD8⁺ T cells, elicits memory responses, and induces both anti-p210 IgM and IgG antibodies to suppress atherosclerosis. Lastly, three intradermal vaccinations of this nanovaccine mitigate the atherosclerosis development in the ApoE^{-/-} mice. Our nanovaccine design and preclinical data thus presents a potential candidate for prophylactic treatment for atherosclerosis.

Atherosclerosis, characterized by the development of lipid-rich plaques in large and medium-sized arteries, is the primary underlying cause of the progression of cardiovascular diseases¹. Evidence indicates that atherosclerosis is an inflammatory disease mediated by both innate and adaptive systems^{2,3}. Therefore, vaccination strategies can be used to treat or prevent the disease. Since Palinski and colleagues conducted the first study on the effects of immunization on atherogenesis with oxidized low-density lipoprotein⁴, various antibody- and cell-based immunotherapies designed to activate B and T cells to clear lipid-rich plaques have been investigated in animal models of atherosclerosis with promising results⁵. Low-density lipoprotein abundance,

particularly the abundance of ApoB, is strongly associated with human atherosclerosis⁶ and are thus candidate antigens for vaccine development^{5,7}. By generating a library of the atheroprotective antigenic epitopes in human ApoB-100, Fredrikson et al. have identified 102 potential epitopes⁸. Among these, p210 has emerged as the prototype antigen for atherosclerotic vaccines due to consistent atheroprotective results^{9–11}.

Cationic bovine serum albumin was previously investigated as a carrier for native p210. Immunization of hypercholesterolemic mice with the p210-albumin complex led to the generation of CD8⁺ T cells¹¹ and regulatory T cells (Tregs)¹², but the antibody responses observed

¹Chemicobiology and Functional Materials Institute, School of Chemistry and Chemical Engineering, Nanjing University of Science and Technology, Nanjing, PR China. ²School of Chemistry and Materials Science, University of Science and Technology of China, Hefei, PR China. ³The First Affiliated Hospital of Nanjing Medical University, Nanjing, PR China. ⁴Department of Cardiology, Nanjing First Hospital, Nanjing Medical University, Nanjing, PR China. ⁵State Key Laboratory of Coordination Chemistry, School of Chemistry and Chemical Engineering, Nanjing University, Nanjing, PR China. ⁶School of Electronic and Optical Engineering, Nanjing University of Science and Technology, Nanjing, PR China. ⁷Institute of Dermatology, Chinese Academy of Medical Sciences and Peking Union Medical College, Nanjing, PR China. ⁸School of Pharmacy, Nanjing Medical University, Nanjing, PR China. ⁹These authors contributed equally: Lei Zhang, Abdulrahman AL-Ammari. ✉e-mail: jazhang618@126.com; wanyingzhu@njmu.edu.cn; sundpe301@163.com

were either minimal or insignificant^{9,11,13}. Nanoparticles are efficient carriers that enhance the density, stability, and bioavailability of antigens and adjuvants to stimulate the activation/maturation of antigen-presenting cells (APCs) that mediate cellular and humoral immune responses^{14–16}. Superparamagnetic iron oxide nanoparticles (SPIONs) are one of the most widely used inorganic nanovaccine materials for cancer immunotherapies, due to their biocompatibility, easy modification, low-cost production, and good immune status^{17–19}. To date, nanovaccine formulation of p210 against atherosclerosis, including incorporation into amphiphile micelles²⁰ or co-delivery with retinoic acid by poly(lactic-co-glycolic acid) nanoparticles²¹, have shown persistent p210-specific immune responses with decreased inflammatory activities and attenuated atherosclerotic lesions. Previous studies suggest p210 does not have biological binding affinity for the mouse MHC-II alleles (I-A^b) but does bind to the MHC-I allele H2K^b²².

Oligodeoxynucleotides containing the unmethylated cytosine-phosphorothioate-guanine motifs (CpG-ODNs) are useful vaccine adjuvants, but suffer from low cellular uptake, are degraded by nucleases, and are subjected to rapid renal clearance. CpG-ODN coating of SPIONs increases cellular uptake of nanoparticles into lysosomes via Class A scavenger receptors (SR-As) and promotes immune cell activation by targeting the TLR9 on lysosomal membranes^{15,23–25}. Concomitant packing of CpG-ODNs and antigens onto nanoparticles enhances the dendritic cell (DC) targeting and immunostimulatory activities of nanovaccines^{26–31}. CpG-ODNs also potentiate DC-mediated activation of class I-restricted T cells³². As scavenger receptor-mediated endocytosis rapidly traffics nanoparticles to lysosomes and results in poor cross-presentation³³, alternative endocytic receptors need to be recruited to traffic antigens to other endosomal compartments and avoid rapid lysosomal degradation.

Recently, Chyu et al. reported that the free p210 peptide preferentially binds to proteoglycans on DC cell surface, suggesting that p210 and CpG-ODNs have different cell uptake mechanisms and different cellular destinations²⁰. We speculated that the different properties of CpG-ODNs and p210 may help to maximize the efficacy of the nanovaccine. Here we tested a nanovaccine prepared from separate conjugation of antigen p210 and adjuvant CpG oligodeoxynucleotides onto superparamagnetic iron oxide nanoparticles and discovered that the ‘cocktail’ vaccine was more effective than SPIONs simultaneously carrying p210 and CpG-ODNs in mouse models. Taken together, the two-pronged delivery of antigen and adjuvant to preferential intracellular destinations represents a promising vaccinology approach for treatment and prevention of atherosclerosis.

Results

Preparation and characterization of SPION-based nanovaccines

We first prepared superparamagnetic iron-oxide nanoparticles grafted to polyethylene glycol (PEG-SPs) by the one-pot thermal decomposition approach³⁴. The particles had a physical core diameter of ~15 nm as shown by transmission electron microscopy (TEM) imaging (Supplementary Fig. 1a); this is smaller than the threshold size necessary for superparamagnetic properties^{35,36}. Compared to the widely adopted co-precipitation approach, the thermal decomposition method generates a hydrophilic carboxyl PEG layer as corroborated by the characteristic Fe-O, C=O, and C-O-C bands in Fourier Transform Infrared (FTIR) spectrum (Supplementary Fig. 1b). The abundant PEG (~85% by weight) enhances the physiological stability of the nanoparticles (Supplementary Fig. 1c)³¹. Using vibrating sample magnetometry (VSM), we observed near-zero remanence for the PEG-SPs and found that their saturation magnetization (M_s) value is 81 emu/(gram of Fe₃O₄) (Supplementary Fig. 1d). The SP-PEG particles have hydrodynamic diameters of around 58.6 nm (Supplementary Fig. 1e).

Next, we covalently conjugated amine-terminated CpG-ODNs and/or p210 to the terminal carboxyl groups on the distal ends of PEG

on the PEG-SPs via carbodiimide crosslinker chemistry to prepare PEG-SPs functionalized with CpG-ODNs (SP-D), with p210 (SP-P), or both at a 1:1 ratio (SP-D1P1) (Fig. 1a). Surface functionalization did not affect the spherical morphology nor did it cause the aggregation as observed by TEM (Supplementary Fig. 1a). Functionalization did increase the mean hydrodynamic diameters (Supplementary Fig. 1e). Demonstrating the successful attachment of negatively charged CpG-ODNs and positively charged p210 peptide, SP-D and SP-P have a higher and lower electrophoretic mobilities than PEG-SPs, respectively (Supplementary Fig. 1f). When the loading ratio of free CpG-ODN and p210 was varied from 2:1 to 1:2, the electrophoretic mobility of the resulting nanoparticles gradually decreased (Supplementary Fig. 1f). In subsequent sections of modulating the nanovaccine by changing the ratio of antigen and adjuvant, SP-D1+P1 and SP-D1P1, especially SP-D1+P1 show potent effect in DC activation/maturation and thus were chosen for animal studies (Fig. 1b). We also quantified the DNA and peptide loadings of SP-D, SP-P, and SP-D1P1 nanoparticles. Based on fluorescence intensities of Cy5-labeled CpG-ODNs after conjugation, the average DNA loadings for SP-D and SP-D1P1 were ~66 and ~75 strands per SPION. Using a bicinchoninic acid assay, we found that the average p210 loadings for SP-P and SP-D1P1 were ~61 and ~112 strands per SPION (Supplementary Fig. 1g).

Antigens and adjuvants promote intracellular delivery of nano-carriers via different mechanisms

Prior to evaluation of uptake of nanoparticles, we measured the effect of the nanoparticles on viability of murine bone marrow derived dendritic cells (BMDCs) during 24-h culture. SP-D had the lowest IC₅₀ value of 1.4 mg/mL, followed by a 1:1 mixture of SP-P and SP-D (SP-D1+P1, IC₅₀ = 2.9 mg/mL) SP-D1P1 (IC₅₀ = 3.5 mg/mL); PEG-SP was the least toxic with an IC₅₀ value of 5.0 mg/mL (Supplementary Fig. 2a). We chose 300 µg/mL as the working concentration for all groups of nanoparticles in subsequent cell studies; under these conditions cell viabilities were higher than 80%.

As evidenced by the iron content of BMDC pellets after 24-h incubation measured by inductively coupled plasma-mass spectrometry (ICP-MS), both CpG-ODN and p210 coatings enhanced cellular uptake (Supplementary Fig. 2b), consistent with previous findings that DNA coating of nanoparticles promotes intracellular delivery^{15,23}. SP-P promoted cellular entry to a lesser extent (~25%) than SP-D, which likely explains the higher toxicity of SP-D compared to other groups. To track the association of different SPIONs with BMDCs, we fluorescently labeled CpG-ODNs and p210 with Quasar 670 and FITC, respectively. Compared to the CpG-ODN and p210 counterparts not tethered to SPIONs, nanoassembly promoted intracellular delivery of both adjuvants and antigens (Supplementary Fig. 2c).

We then tracked the SPIONs as a function of time by confocal microscopy. During the first 8 h of incubation, all types of particles enter BMDCs in a time-dependent manner as indicated by a gradual increase in fluorescence intensity (Supplementary Fig. 3a and Supplementary Fig. 3b). The fluorescence due to all types of particles decreased from 8 to 24 h, probably due to the degradation of DNA and peptide inside acidic cellular compartment such as late endosomes or lysosomes, which have been reported by previous studies including ours^{31,37,38}. We also evaluated the intracellular retentions of CpG-ODN and p210 on SP-D1P1 by tracking the co-localization of Quasar 670 and FITC fluorescence. A consistent Pearson's coefficient of ~0.8 was observed from 1 h to 16 h after incubation (Supplementary Fig. 3c), suggesting that both CpG-ODN and p210 remained on SPIONs during incubation. In contrast, the Pearson's correlation coefficient of Quasar 670 and FITC fluorescence signals from SP-D1+P1 was much lower and varied over time (Supplementary Fig. 3d), strongly suggesting that the mechanisms of endocytosis of SP-D and SP-P differ.

Spherical nucleic acids (SNA)^{15,23} and SNA-like nanoparticles³¹ enhance cellular uptake by associating with the SR-A. Supporting the

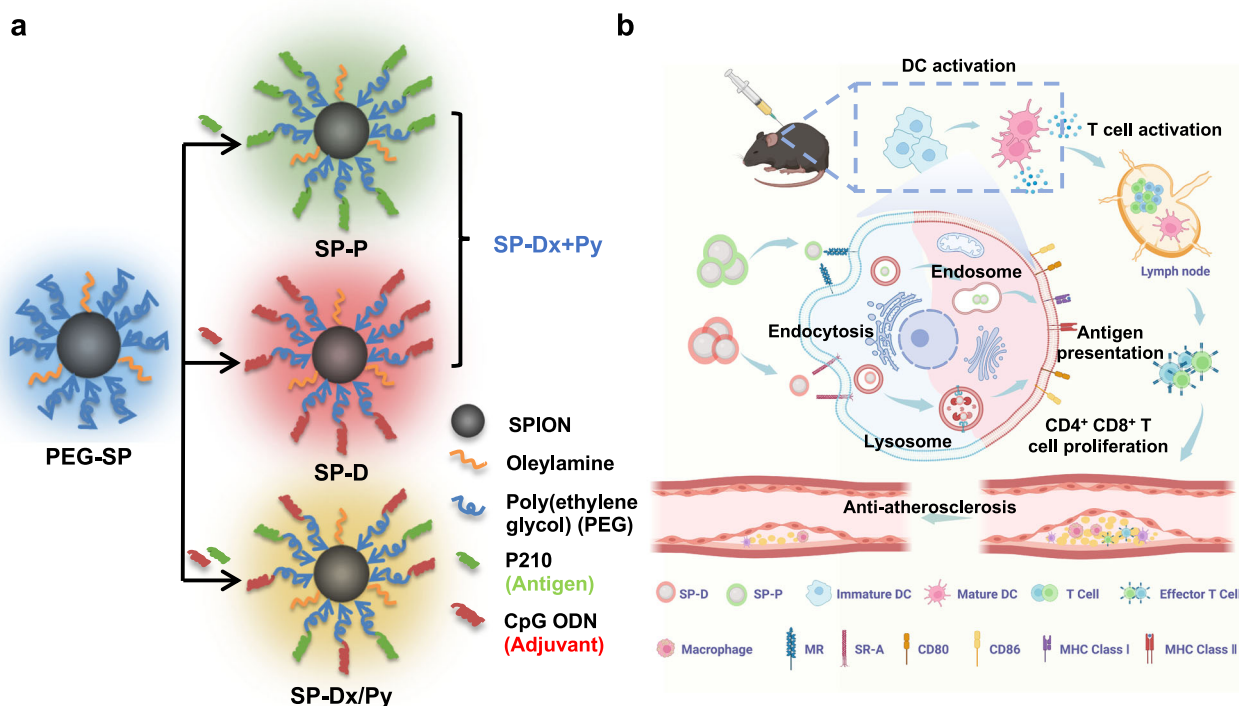


Fig. 1 | Preparation, intracellular delivery, and mechanism of SPION-based nanovaccines. a Schematic illustration of preparation of SPIONs functionalized with CpG-ODN (SP-D), with p210 (SP-P), and both (SP-DxPy, where x and y represent the ratio between CpG-ODN and p210 added to the reaction). **b** Illustration of the

nanovaccine cocktail SP-D1 + P1 showing enhanced DC activation by endocytosis via SR-A and MR for adjuvant and antigen uptake, promoting both cellular and humoral immune responses, and exerting potent anti-atherosclerosis effects. Created with BioRender.com. Han, Y. (2025) <https://BioRender.com/l23k764>.

hypothesis that these receptors are important for uptake of nanoparticles functionalized with CpG-ODN, we observed reductions in fluorescent intensity for SP-D, SP-D1P1, and SP-D1 + P1 (as measured by the intensity of Quasar 670-labeled CpG-ODN) of 92%, 93%, and 95% in cells pre-treated with fucoidan, a competitive ligand of SR-A (Fig. 2a, b)³⁹. In cells incubated with SP-P and SP-D1 + P1 functionalized with FITC-labeled p210, fucoidan inhibited uptake by 39% and 55%, respectively. Pre-treatment with amiloride, a blocker of macropinocytosis, reduced the uptake of SP-P by 62%. Pre-treatment with mannan, an inhibitor of phagocytosis mediated by the mannose receptor (MR), reduced the uptake of SP-P and SP-D1 + P1 by 92% and 84%, respectively. These results suggest that the uptake of p210-coated nanoparticles is largely mediated by macropinocytosis and mannose receptor-mediated endocytosis. The uptake of SP-D1 + P1 appears to occur through both SR-A and MR-mediated endocytosis, judging from the intensities of the two components.

We also evaluated the intracellular fates of the nanovaccines in cells treated with Lysotracker dye (Fig. 3a). Since the signals from antigen and adjuvant co-localize well in SP-D1P1 (Supplementary Fig. 3c), we only tracked Quasar 670-labeled CpG-ODN in SP-D1P1. By analyzing the co-localization coefficients, we discovered that SP-D and SP-D1P1 begin to co-localize with lysosomes between 4 and 8 h after addition of the SPIONs to cells (Fig. 3b). In contrast, SP-P was not co-localized with lysosomes until after 16 h of incubation. Separate tracking of antigens and adjuvants in SP-D1 + P1 revealed that co-localization of SP-P with Lysotracker dye lagged that of SP-D (Fig. 3c). The lagged uptake of SP-P may also be caused by the down-regulation of MR after DC activation⁴⁰, which exhibited a slower rate of intracellular accumulation (Supplementary Fig. 3b). The Pearson's coefficients between the SPION labels of SP-D, SP-D1P1 and SP-P and the Lysotracker dye in all decreased after 24 h, which could be due to the degradation of DNA and peptide in acidic compartments. We cannot rule out the possibility that endosomal or lysosomal

escape occurs as this has been observed for SNAs⁴¹. Recently, the significance of endocytosis-dependent routing into distinct endosomal compartments for antigen presentation has been demonstrated; MR-internalized antigens are known to traffic to early endosomes, a primary process involved in cross-presentation onto MHC I molecules, leading to the activation of CD8⁺ T cells^{33,42,43}. Since p210 is known to bind to the mouse MHC-I allele H2K^b²², we speculated that SP-D1 + P1 would induce CD8⁺ T cell immune responses.

Nanovaccines activate DCs and promote cytokine secretion in vitro

We investigated APC activation levels when stimulated by the prepared nanovaccines in vitro. BMDCs were incubated with SP-D1P1, SP-D1 + P1, a physical mixture of antigen and adjuvant (D + P), or antigen or adjuvant alone. Cells were treated with 300 µg/mL SP-D1P1 and SP-D1 + P1, corresponding to 490 nM CpG-ODN and 732 nM p210 in SP-D1P1 and to 432 nM CpG-ODN and 399 nM p210 in SP-D1 + P1, based on previously determined loadings. We used free CpG-ODN and p210 at 500 nM for comparisons, which were at similar concentrations of the components in the nanovaccines. The nanoparticles or molecules were incubated with BMDCs for 24 h or 72 h and then analyzed by flow cytometry. The DC population was defined as CD11c⁺ cells and the upregulation of costimulatory surface markers (CD86 and CD80) and MHC I and MHC II were evaluated (Fig. 4a). SP-D1 + P1 upregulated CD86, MHC I, and MHC II to 26.0%, 21.3%, and 30.0% after 24 h of incubation, whereas the mixture of adjuvant and antigen not bound to nanoparticles (D + P) resulted in upregulations of 19.8%, 9.93%, and 24.2, respectively (Fig. 4b–d). The expression of CD80 was not significantly upregulated until after 72 h (Supplementary Fig. 4a and Supplementary Fig. 4b). BMDC maturation appears to be due mainly to the adjuvant as SP-D enhanced the expression of CD86, MHC I, and MHC II, although to a lesser extent than SP-D1 + P1 (Fig. 4b–d). The free

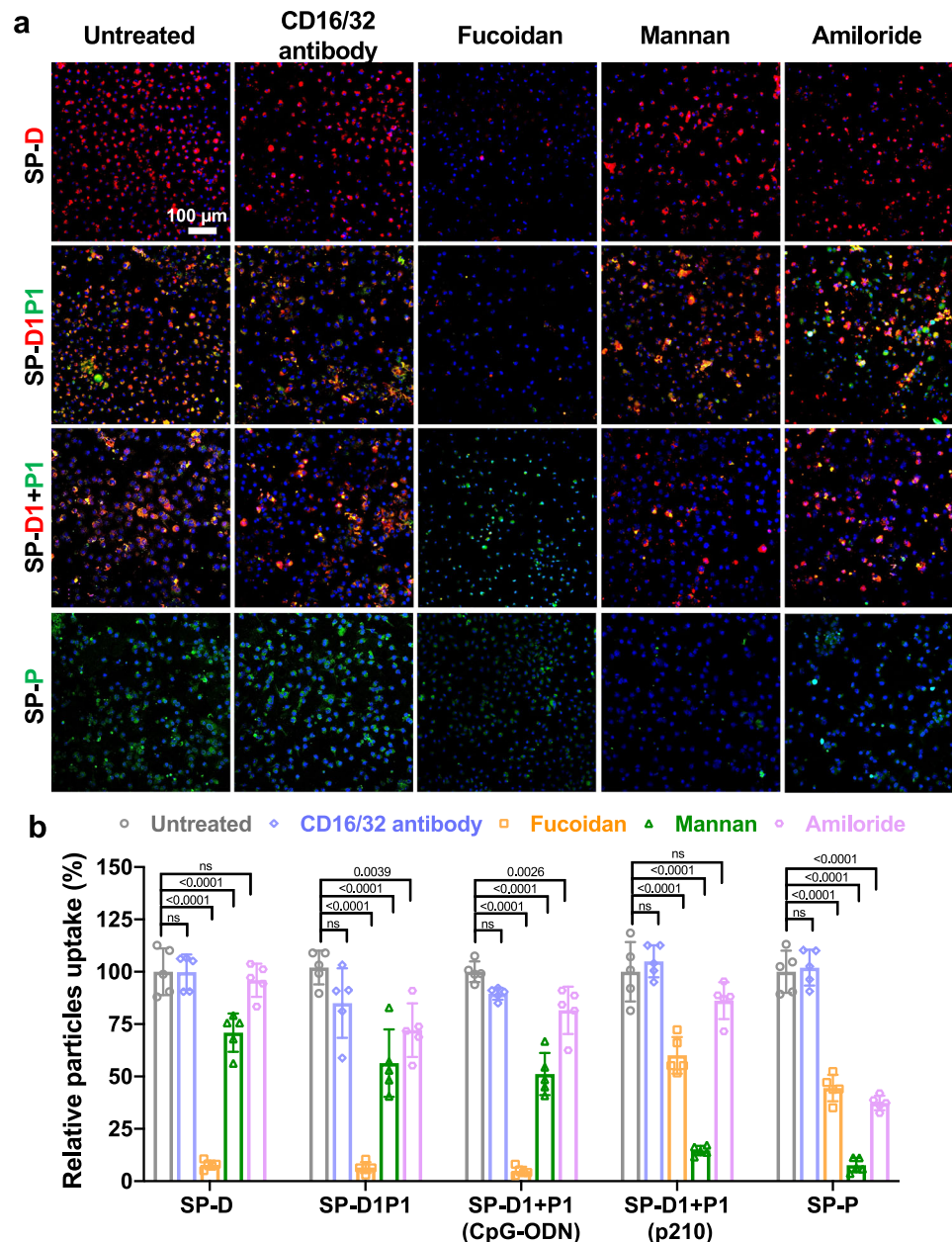


Fig. 2 | Mechanisms of cellular uptake of SPION-based nanovaccines in BMDCs. **a** Representative confocal images of BMDCs treated with anti-CD16/32 antibody, fucoidan, mannan, or amiloride incubated with SP-D, SP-D1P1, SP-D1 + P1, and SP-P for 4 h. CpG-ODN was Quasar 670-labeled (red) and p210 was FITC-tagged (green). Nuclei were stained with Hoechst 33342 (blue). **b** Statistical analysis of the

fluorescent intensities after different treatments. $n = 5$ individual experiments and data are presented as mean \pm SD. One-way ANOVA with Dunnett's *post hoc* test used to determine significance versus the untreated group. Statistically significant p values are reported; ns mean no significance. Source data are provided as a Source Data file.

CpG-ODN was less potent than SP-D (Fig. 4b-d), likely due to lower levels of uptake as shown above. SP-D1P1 was not as potent as SP-D1 + P1 at 24 h of incubation but was a more persistent activator, for it increased the expression levels of CD86, MHC I, and MHC II even after 72 h (Supplementary Fig. 5, Supplementary Fig. 6a and Supplementary Fig. 6b). Interestingly, although iron oxide nanomaterials are known to induce pro-inflammatory immune responses and act as self-adjuvants^{18,44,45}, which motivated us initially to use SPIONs as the antigen/adjuvant carriers, we note that PEG-SPs may have immune inhibitory effects on BMDCs, as the expression of the surface markers generally decreased compared to untreated cells (Fig. 4b-d).

We collected BMDC cell supernatants after 24 h of incubation with nanovaccine preparations to quantify cytokine secretion by enzyme-linked immunosorbent assay (ELISA). IL-12p70, IL-6, and TNF- α were

quantified. Cytokine expressions were considerably upregulated by treatment with SP-D1P1, SP-D1 + P1 as well as SP-D (Fig. 5a). Specifically, the IL-12p70 secreted by BMDCs incubated with SP-D1P1 and SP-D1 + P1 was 130 and 242 pg/mL, 3-fold higher than that of BMDCs incubated with the physical mixture of D + P or with CpG-ODNs (Fig. 5a). IL-12 plays a vital role as a licensing cytokine, driving the polarization of activated CD4⁺ T cells towards a Th1 phenotype. This polarization is instrumental in facilitating the generation of robust cytotoxic T lymphocyte responses⁴⁶. The high amount of IL-12p70 secreted by BMDCs incubated with SP-D1P1 and SP-D1 + P1 pulsed BMDCs suggest that these preparations should induce CD8⁺ T cell responses. The IL-6 content in cell supernatants was similar among all treatments that included the CpG-ODN adjuvant (Fig. 5b), but the TNF- α concentration was higher in cell supernatants of cells treated with SP-D1P1 and

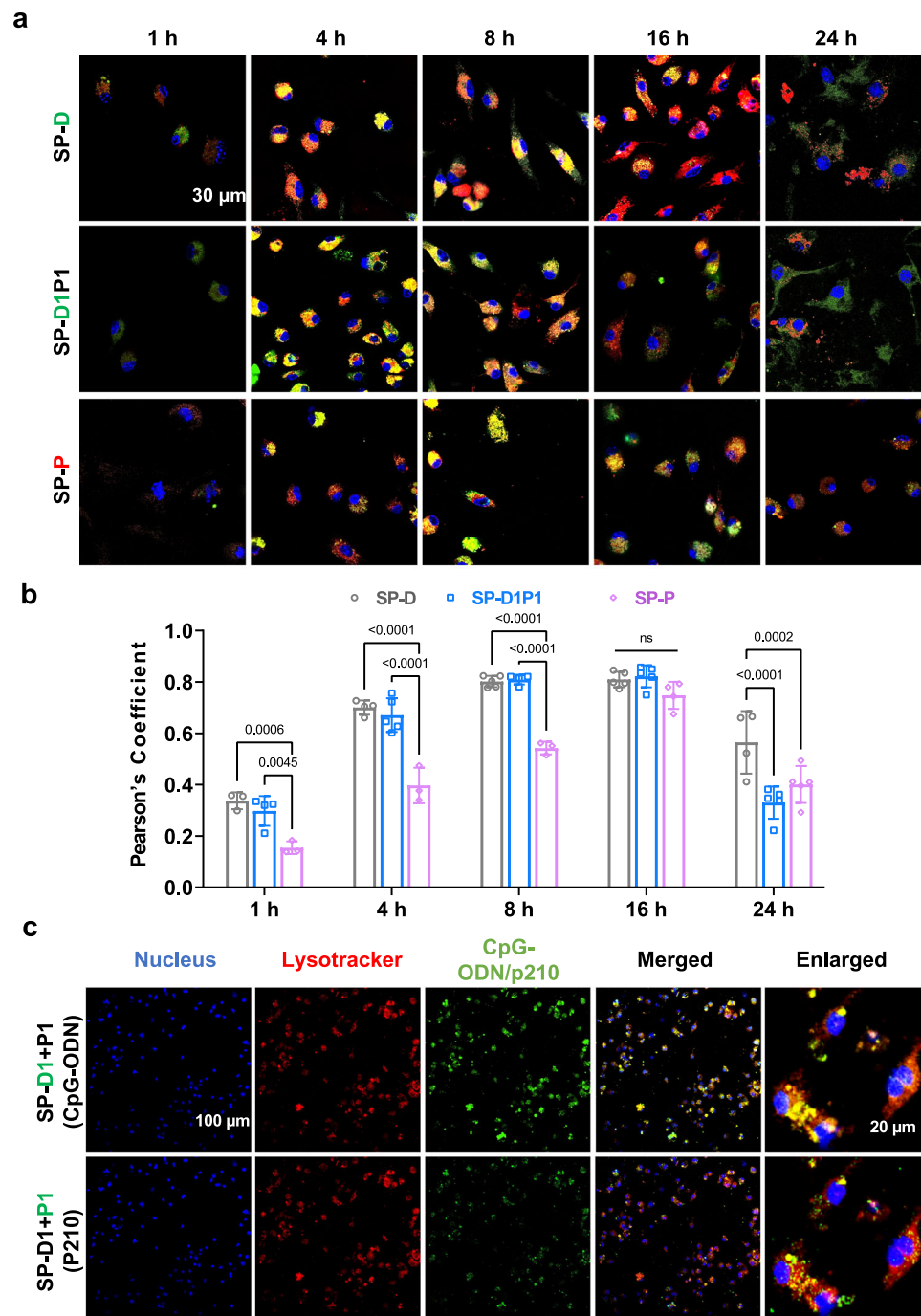


Fig. 3 | Intracellular trafficking of nanoparticles revealed by co-localization with Lysotracker dye. a Confocal microscopic images of BMDCs incubated with SP-D (green), SP-D1P1 (green), and SP-P (red) and counter-stained with Lysotracker dye to mark lysosomes (shown in either red for SP-D and SP-D1P1 or green for SP-P). Nuclei were counterstained with Hoechst 33342 (blue). **b** Pearson's correlation coefficients for co-localization of SPION with Lysotracker dye as a function of time for SP-D ($n = 3$ for 1 h, $n = 4$ for 4 h and 24 h, $n = 5$ for other time points), SP-D1P1 ($n = 4$ for 1 h and 6 h, $n = 5$ for other time points), and SP-P ($n = 4$ for 24 h, $n = 3$ for other time points). Pearson's correlation coefficient of 0.7 or above indicates

substantial colocalization. The replicates are from individual experiments and data are presented as mean \pm SD. Statistical significance at each time point was calculated using one-way ANOVA with Tukey's *post hoc* test and p value was indicated; ns means no significance. **c** Representative confocal microscopy images of BMDCs after 4-h incubation SP-D1 + P1, prepared with fluorescently tagged adjuvant or antigen (indicated in green) and counter-stained with Lysotracker dye (red); yellow signals reflect co-localization ($n = 3$ individual experiments). Nuclei were counter-stained by DAPI (blue).

SP-D1 + P1 (Fig. 5c). Free p210, SP-P, and the carrier PEG-SP did not promote cytokine secretion compared to untreated cells, confirming the role of the adjuvant in DC activation/maturation.

We next evaluated the effect of the loading ratio between CpG-ODN and p210 antigens. During the conjugation of CpG ODNs and p210 to SPION, the molar ratios of the initial free DNA and peptide

were adjusted to prepared SP-D2P1, SP-D1P1, and SP-D1P2, which have ratios of adjuvant to antigen of 2:1, 1:1, and 1:2, respectively. We also prepared mixtures SP-D2 + P1, SP-D1 + P1, and SP-D1 + P2 at these same ratios. In flow cytometric analysis for MHC I, MHC II, co-stimulatory signals, and cytokines secreted after 24 h of incubation, we did not find significant differences resulting from differences in ratios of adjuvant

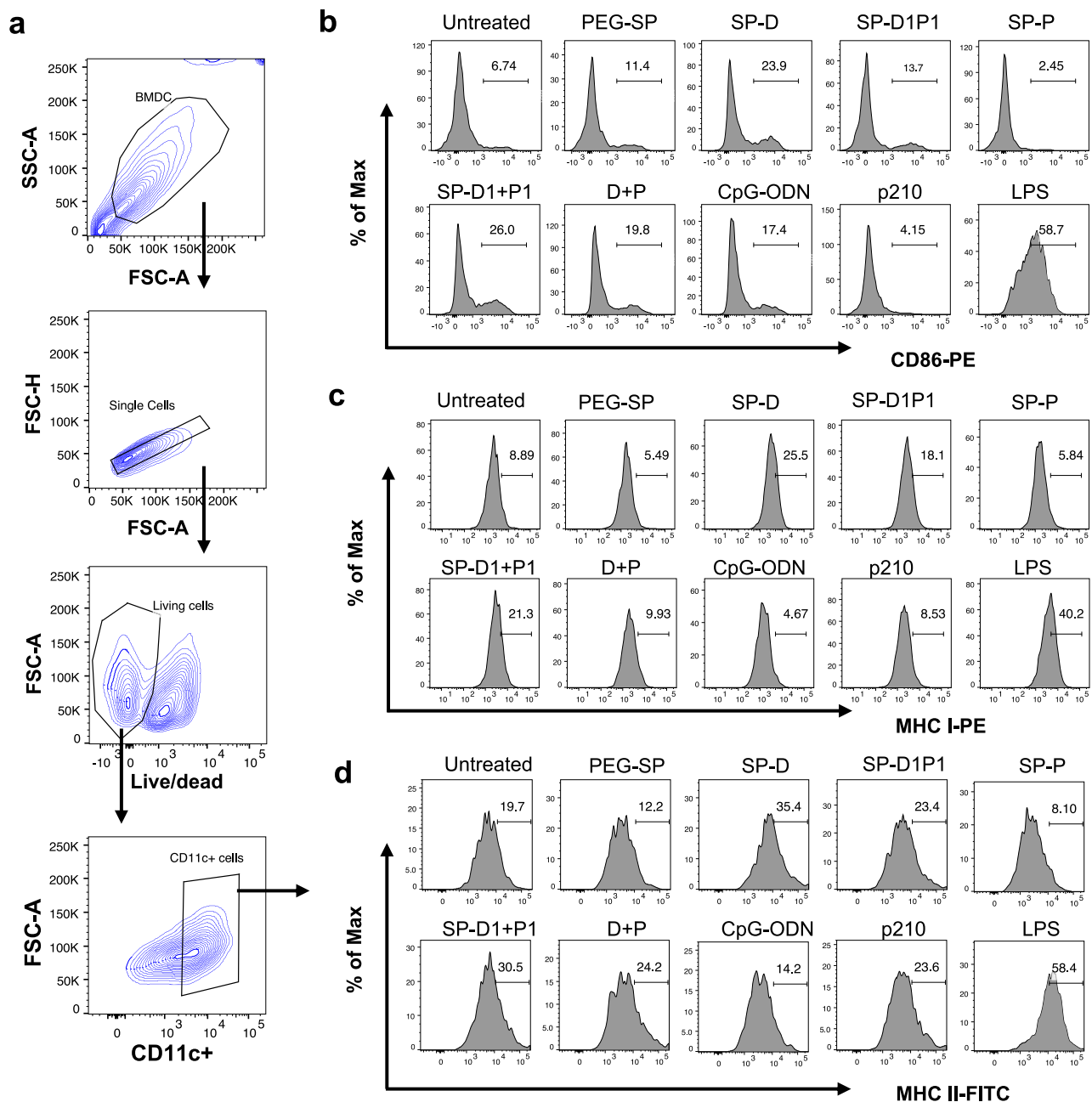


Fig. 4 | Vaccine formulations for optimized BMDC activation. **a** Viable BMDCs were identified based on light scattering properties, live/dead staining, and CD11c fluorescence using FACS analysis. Antibody staining for CD86 (**b**), MHC I (**c**), and MHC II (**d**) expression with indicated preparations for 24 h. Representative FACS

analyses are shown ($n = 3$ individual experiments). This gating was also used to generate FACS data shown in Supplementary Figs. 4–7. Source data are provided as a Source Data file.

to antigen (Supplementary Fig. 7). Therefore, SP-D1P1 and SP-D1 + P1 were used in subsequent experiments.

Nanovaccines promote functional T cell responses in cell culture

Functional assays of DC responses in vitro were also conducted to confirm the CD8⁺ T cell responses induced by our two-pronged nanovaccination strategy. BMDCs treated with nanoparticle preparations SP-D1P1 and SP-D1 + P1 and controls PEG-SP, SP-P, and the combination of adjuvant and antigen were co-cultured with autologous splenocytes labeled with carboxyfluorescein succinimidyl ester for 4 days before proliferation analysis by flow cytometry (Supplementary Fig. 8). All treated groups show decreased proportions of CD8⁺ T cells relative to all CD3⁺ T cells compared to the untreated group, and treatment with SP-D1P1 and SP-P resulted in a much lower percentage

of CD8⁺ T cells (Fig. 5d). These results can be explained by the different proliferation patterns. CD8⁺ T cells proliferated under the no treatment condition and upon treatment with PEG-SP, D + P, and SP-D1 + P1 (Supplementary Fig. 9a), whereas CD4⁺ T cell expansion was observed upon treatment with SP-D1P1 and SP-P (Fig. 5e and Supplementary Fig. 9b).

As the memory phenotype cells (CD44⁺), especially the effector and/or effector memory cells in the spleen⁴⁷, proliferate after immunostimulation^{48,49}, we evaluated CD44 and CD62L markers. The expansion of CD8⁺ cells in D + P and SP-D1 + P1 groups could indeed be attributed to the proliferation of effector and/or effector memory T cells. The percentages of CD44⁺CD62L⁺ cells relative to all CD8⁺ cells were 77.65% and 75.43% for D + P and SP-D1 + P1 groups, significantly higher than the untreated (56.97%) and PEG-SP-treated

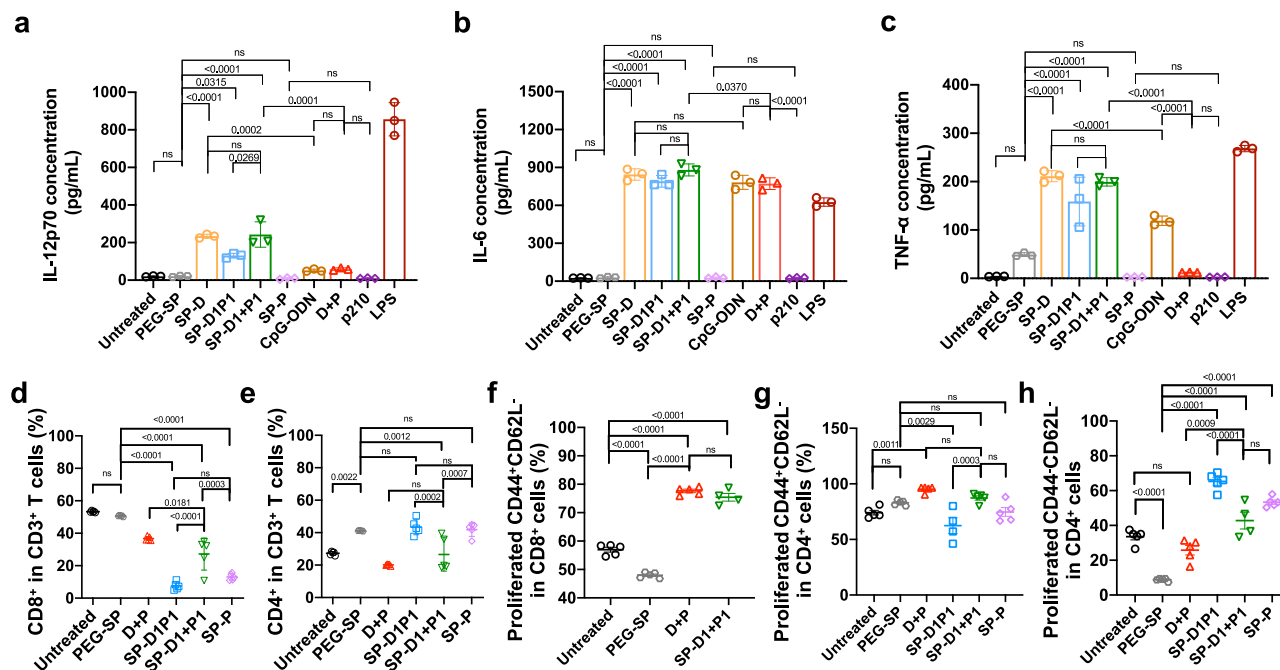


Fig. 5 | Cytokine secretion by and functional analyses of BMDCs treated with SPION preparations. **a–c** After incubation with indicated adjuvant and antigen preparations for 24 h, the BMDC supernatants were collected and IL-12p70 (**a**), IL-6 (**b**), and TNF-α (**c**) were quantified by ELISA. Data are presented as mean ± SD ($n = 3$ samples per group). Statistical significance was calculated using one-way ANOVA followed by Tukey's multiple comparisons test. **d–g** BMDCs treated as indicated were co-cultured with splenocytes for 4 days and percentages of CD8⁺

cells in CD3⁺ T cells (**d**), CD4⁺ cells in CD3⁺ T cells (**e**), CD44⁺CD62L⁻ in CD8⁺ T cells (**f**), CD44⁺CD62L⁻ in CD4⁺ T cells (**g**), and CD44⁺CD62L⁻ in CD4⁺ T cells (**h**) were determined. Data are presented as mean ± SD ($n = 5$ samples per group except that $n = 4$ for SP-DI + P1 in (**f**, **h**), $n = 4$ for SP-DIPI in (**g**). Statistical significance was calculated using one-way ANOVA followed by Tukey's multiple comparisons test. Significant p values were indicated; ns means no significance. Source data are provided as a Source Data file.

(47.97%) groups, whereas few CD8⁺ effector and/or effector memory T cells were detected upon treatment with SP-DIPI and SP-P (Fig. 5f). No treatments altered the proliferation of CD4⁺ effector and/or effector memory T cells with the exception of a slight decrease induced by SP-DIPI (Fig. 5g). Interestingly, expansion of the CD4⁺ T cells in the presence of SP-DIPI and SP-P were attributed to proliferation of CD44⁺CD62L⁻ cells (Fig. 5h), a poorly characterized cell population. These data suggest that SP-DI + P1 and SP-DIPI have different activation mechanisms. Cytokine profiling revealed that nanovaccines enhanced levels of IFN-γ and IL-17 and decreases levels of IL-10 and IL-4 (Supplementary Fig. 10a–d). Taken together, these *in vitro* experiments show that the two-pronged uptake of antigens and adjuvants promote CD8⁺ effector and/or effector memory T cell proliferation. These could be the effector cells in the atheroprotective immunomodulation.

Nanovaccines traffic to lymph nodes and activate DCs in mice

To investigate the lymph node retention of the nanovaccines, C57BL/6 mice were given subcutaneous injections of PBS, D + P, SP-DIPI, SP-DI + P1, or SP-P in the dorsal area between the scapula (Fig. 6a). At 20, 48, and 72 h post-injection, we collected brachial lymph nodes and inguinal lymph nodes from the animals and compared their sizes. Treatment with all preparations except SP-P resulted in at least one visibly enlarged brachial or inguinal lymph node at 20 h with generally decreased sizes at 72 h (Supplementary Fig. 11a). Prussian blue staining of sectioned lymph nodes also suggested drainage of SP-DIPI, SP-DI + P1, and SP-P groups at 20 h as indicated by Prussian blue staining in the subcapsular space by afferent lymphatic vessels (Fig. 6b). This staining was significantly decreased at 48 h and was not observed at 72 h (Supplementary Fig. 11b). We also noted an increase in DCs (CD11c⁺) and infiltration of T lymphocytes (CD3⁺) in lymph nodes of mice treated with in SP-DIPI and SP-DI + P1 at 20 h, which was decreased at 72 h (Supplementary Fig. 12). These observations indicate

that retention of the nanovaccines peaks in lymph nodes peaks at 20 h post-injection.

In another experiment, we used fluorescently-labeled CpG-ODNs and p210 for nanovaccine preparation and collected the draining lymph nodes at 20 h for cellular level analysis after a single subcutaneous injection of various preparations. Fluorescence imaging confirmed the presence of TAMRA-labeled p210 and Quasar 670-labeled CpG-ODNs in at least one brachial or inguinal lymph node from mice treated with D + P, SP-DIPI, SP-DI + P1, and SP-P (Fig. 6c). Enlargement of draining lymph nodes was again observed in mice treated with D + P, SP-DIPI, and SP-DI + P1 but not SP-P (Fig. 6c).

We then digested the lymph nodes and used flow cytometry to quantify DCs that were positive for FITC-labeled p210 (FITC⁺CD11c⁺). Mice treated with SP-DIPI, SP-P, and SP-DI + P1 had higher FITC⁺ DC populations than did mice treated with PBS or with D + P (Fig. 6d), suggesting less cellular uptake of D + P despite the obvious dLN retention in Fig. 6c. Immunofluorescence staining of the lymph node sections showed obvious co-localization and/or close contact between TAMRA(p210)/Quasar 670 (CpG-ODN) signals and DCs in mice treated with SP-DIPI, SP-P, and SP-DI + P1, and co-localization was also observed between TAMRA/Quasar 670 and macrophages (Fig. 6e). Co-localization was observed to a lesser extent in mice treated with D + P (Fig. 6e). In mice treated with SP-DIPI, the Quasar 670 signals from the tagged CpG-ODNs largely co-localized with TAMRA signal from the labeled p210 in SP-DIPI, whereas this was not always the case in mice treated with D + P and SP-DI + P1 (Fig. 6e).

Analyses using inductively coupled plasma optical emission spectrometry (ICP-OES) to detect iron levels revealed no significant trafficking of SPIONs to the organs such as heart, liver, kidney, pancreas, or brain in mice treated with any of the preparations (Supplementary Fig. 13a). However, SP-P showed higher retention in the lungs than did the other preparations (Supplementary Fig. 13a). We then tracked the antigens and adjuvants separately by fluorescence

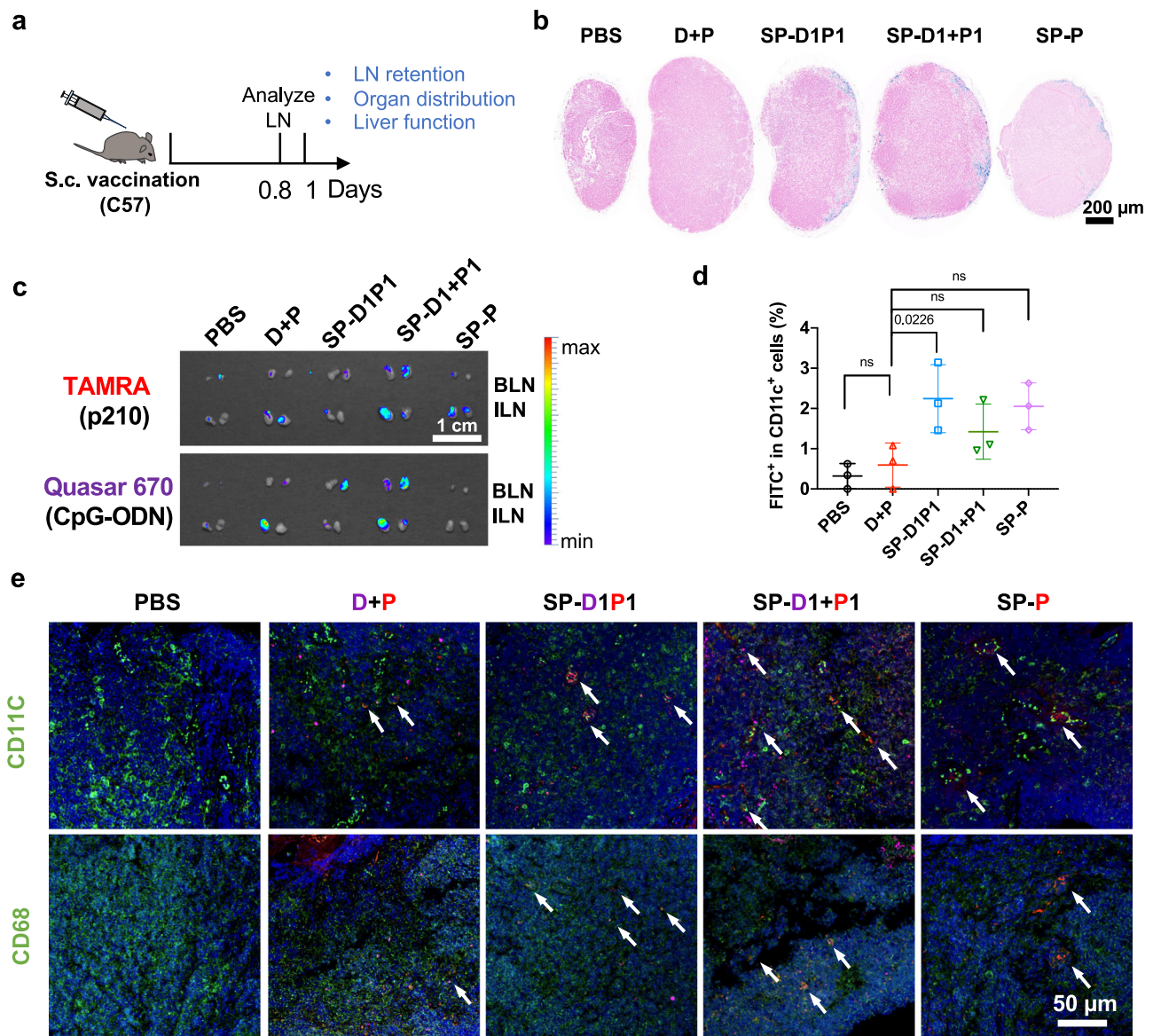


Fig. 6 | SPION-based nanovaccines promote lymph node retention, DC uptake, and interactions with macrophages. a Schedule for one-dose subcutaneous injection of C57BL/6 mice. **b** Representative photographs of draining lymph nodes excised 20 h after vaccination with indicated preparations, separately merged with fluorescence signals from the nanovaccines formulated with TAMARA-labeled p210 or Quasar 670-labeled CpG ODNs ($n = 3$ individual experiments). **c** Prussian blue staining of sectioned brachial lymph nodes (BLN) and inguinal lymph nodes (ILN) excised at 20 h post vaccination ($n = 3$ individual experiments). **d** Flow cytometric analyses of FITC-labeled p210 in DC cells (CD11c⁺) from draining lymph nodes of mice treated with the indicated preparations. The data are presented as mean \pm SD

($n = 3$ mice per group). Statistical significance was calculated via one-way ANOVA with Dunnett's *post hoc* test versus the D + P group. Statistical significant p values were reported; ns means no significance. **e** Representative images of lymph nodes from C57BL/6 mice treated with one dose of Quasar 670-labeled CpG-ODNs (purple) and TAMRA-labeled p210 (red) nanovaccines. DCs and macrophages were immunofluorescently stained for CD11c and CD68, respectively (green). Nuclei were counterstained with DAPI (blue). White arrows in the representative images indicate co-localization between or close contact of the vaccines and DCs or macrophages. $n = 3$ individual experiments in each treatment group. Source data are provided as a Source Data file.

imaging. CpG-ODN signals (Quasar 670) from D + P were detected in all the organs except brain, whereas the CpG-ODN signal from SP-D1P1 and SP-D1 + P1 were detected mostly in blood serum, livers and kidneys (Supplementary Fig. 13b). Interestingly, we saw obvious retention of TMARA-labeled p210 in lung and serum in SP-P group, consistent with the ICP-OES data, suggesting antigen transferring to the blood, which was not seen in mice treated with D + P or SP-D1P1 (Supplementary Fig. 13b). By tracking the fluorescence intensities in vivo at injection sites from 4 h to 168 h after injection, we found that D + P had a longer half-life, particularly for the adjuvant, at the injection site than other preparations (Supplementary Figs. 14–18).

Of note, the nanovaccines did not cause liver toxicity, as the serum liver function markers at 20 h post the injection and at week 13 after full vaccination did not show abnormalities in albumin, alanine transaminase, and aspartate transaminase levels (Supplementary Fig. 19a, b). Moreover, bodyweights of vaccinated mice were not significantly different from those of mice injected with PBS at week 13 (Supplementary Fig. 19c).

We also evaluated the effects of two subcutaneous injections of vaccines on DCs in draining lymph nodes of ApoE^{-/-} mice at week 13 (one week after the second booster). Flow cytometric analysis showed that both CD11c⁺ and CD11c⁺CD86⁺ DC populations in mice treated with SP-D1 + P1 were increased slightly compared to the other groups

(Supplementary Fig. 20a–c), suggesting that this preparation stimulated DC maturation in the draining lymph nodes more effectively than did other preparation. These data suggest that nanoformulation of antigens and adjuvants reduces unwanted distribution to organs like heart and lungs, enhances the draining lymph node targeting, and better activates DCs in draining lymph node, which is a prerequisite for the atheroprotective immune responses.

SPION-based nanovaccines alleviate atherosclerotic plaque development

We next examined the atheroprotective effects of nanovaccines in the ApoE^{-/-} mouse models. Mice were fed on a standard chow diet and were given a primary subcutaneous immunization with D + P, SP-D1P1, SP-D1 + P1, or SP-P at 7 weeks of age, followed by two boosters at 9 and 12 weeks of age; control mice were injected with PBS on the same schedule (Fig. 7a). One week after the last booster, mice were switched to a high-cholesterol diet for 14 weeks, which was previously shown to result in development of atherosclerotic plaques⁵⁰. We first evaluated the atheroprotective effect of vaccinations by staining whole aortas (Fig. 7b, c) and aortic root sections (Fig. 7d) with Oil Red O (ORO). The percentages of lesion areas in the whole aortas from mice treated with SP-P, D + P, SP-D1P1, and SP-D1 + P1 were all significantly lower than the percentages of PBS group. SP-D1 + P1 showed the most potent efficacy with an overall reduction in lesion area by ~55% compared to PBS treatment (Fig. 7d). SP-D1P1 was slightly less effective but was more effective than SP-P or D + P. The areas of lesions within the mice's aortic roots in the SP-D1 + P1 group were significantly smaller compared to those from the PBS, D + P, SP-D1P1, and SP-P groups, with ~58% smaller lesion areas for SP-D1 + P1-treated mice than untreated mice (Fig. 7d). We then examined the effect of the vaccines on the plaque stabilization by quantifying the collagen-expressing areas, as low collagen content is linked to atherosclerotic plaques that are prone to rupture⁵¹. Masson's trichrome staining of aortic root sections revealed a notably thicker collagen cap surrounding the plaques in the SP-D1 + P1 group compared to all other groups (Fig. 7e).

We also investigated the inflammatory cell types in the aortic root. ICAM-1, CD68, and CD11c are the markers of inflammatory endothelial cells, macrophages, and DCs, respectively. The weakest signals for all three cell types were observed in aortic roots of mice treated with SP-D1 + P1. Statistical analysis showed the aortic CD68⁺, CD11c⁺, and ICAM-1-positive areas for the SP-D1 + P1 mice were 49.5%, 41.1%, and 43.2% smaller respectively, than these areas in mice treated with PBS (Fig. 7f–h). SP-D1P1 was less effective than SP-D1 + P1 but still induced a significant reduction compared to PBS (Fig. 7f–h).

The effect of nanovaccines on the plasma cholesterol levels were also evaluated by measurement of the total cholesterol, low-density lipoprotein cholesterol, high-density lipoprotein cholesterol, and triglyceride in serum of vaccinated ApoE^{-/-} mice at 26 weeks (Supplementary Fig. 21a). Although a previous p210-related immunization strategy was shown to reduced serum cholesterol²⁰, which suggests interactions between immune responses and cholesterol metabolism⁵², we did not observe significant differences between vaccinated and control groups.

None of the vaccine preparations affected the bodyweight in this experiment (Supplementary Fig. 21b). Moreover, our nanovaccines did not impact the histological structures of the major organs of the ApoE^{-/-} mice at 26 weeks (Supplementary Fig. 22). Despite some residual iron in the skin close to injection sites (Supplementary Fig. 23), inductively coupled plasma-mass spectrometry measurements of the major organs did not show significant differences in terms of iron contents between vaccinated mice and mice given PBS (Supplementary Fig. 24), suggesting that the vaccination strategy did not pose an extra iron burden due to biodegradation of the iron oxide nanoparticles. Together, these data suggest that the

SP-D1 + P1 preparation had optimal atheroprotective effects of the preparations tested and that the vaccines are biocompatible.

Antibody responses to nanovaccine immunization

In studying the vaccinations against atherosclerosis, an ongoing challenge is deciphering the mechanism of action, a prerequisite for translation of a vaccination protocol to humans. Regulatory T cells, CD8⁺ T cells, and antigen-specific IgG may confer atheroprotective effects, depending on the administration form, adjuvant type, dose, or route of delivery^{53,54}. The induction of p210-specific antibodies has been reported in studies using complete/incomplete Freund's adjuvant⁵⁵, and using Pan-DR T cell epitopes peptide and alum as carrier and adjuvant, respectively⁵⁶. Although recent studies suggest atheroprotection does not require IgG antibodies⁵⁷, we measured the IgM and IgG levels against p210 in immunized ApoE^{-/-} mice both at 10 weeks and 26 weeks of age. Levels of serum IgM and IgG levels against p210 increased by at least 4 folds compared to the PBS-treated mice at both time points for mice treated with D + P, SP-D1P1, and SP-D1 + P1 (Fig. 8a, b). The significant increase in both IgM and IgG at 10 weeks (one week after the primary booster) suggested that the immunoglobulin class switching had already occurred in response to the nanovaccines. At week 26, immunization with SP-D1 + P1 resulted in the higher levels of both antibodies than did SP-D1P1 or D + P. Consistent with a previous study¹¹, PBS treatment also led to a significant increase in p210 IgM titer at 26 weeks compared to that at 10 weeks age, suggesting an immune response against endogenous p210 in the ApoE^{-/-} mice. To exclude this factor, we measured IgM and IgG levels against p210 in C57BL/6 mice fed a standard chow diet at 10 weeks and 15 weeks following the same vaccination protocol. Vaccination enhanced both IgM and IgG levels at 10 weeks of age in the C57BL/6 mice and vaccination with SP-D1 + P1 resulted in higher levels of antibodies than other preparations (Supplementary Fig. 25a, b). Taken together, these experiments indicate that vaccination with CpG-ODNs and p210 induces specific humoral responses within a week after the primary booster and that SP-D1 + P1 leads to the highest level of antibody titers of the preparations tested.

Nanovaccine immunization elicits both CD4⁺ and CD8⁺ T cell-mediated immune responses

Given that our nanovaccines were expected to result in CD8⁺ T cell immune responses, we evaluated the responses of CD8⁺ T cells of ApoE^{-/-} mice to our immunization protocols. One week after the first booster, splenocytes were collected and subjected to flow cytometric analysis (Supplementary Fig. 26). Previously, increases in CD8⁺CD25⁺ T cells were observed in ApoE^{-/-} mice early after p210 immunization¹¹, and immunomodulatory functions of CD4⁺CD25⁺ regulatory cells were reported to reduce atherosclerosis⁵⁸. We did not detect any significant difference in the percentage of splenic CD8⁺ or CD8⁺CD25⁺ cells between mice vaccinated with D + P, SP-D1P1, or SP-D1 + P1 or controls injected with PBS (Fig. 8c, d), but the CD8⁺IL-10⁺ population was detected at much higher levels in the SP-D1 + P1-treated group than in the other three groups (Fig. 8e). Although the IL-10-secreting CD8⁺ T cells have not been linked to the development of atherosclerosis, they are known to be a suppressor T cell lineage^{59,60}.

Flow cytometric analysis also showed no significant differences between the percentages of splenic CD8⁺CD62L⁺ cells among groups (Fig. 8f). Vaccination with D + P slightly enhanced the percentage of CD8⁺ central memory cell (CD8⁺CD44⁺CD62L⁺) compared to the other groups (Fig. 8g). Both SP-D1P1 and SP-D1 + P1 significantly increased the percentage of CD8⁺ effector memory cells (CD8⁺CD44⁺CD62L⁻) by about 5% compared to PBS and D + P groups (Fig. 8h). These results suggest the establishment of immunological protection by the memory cytotoxic T lymphocytes in mice vaccinated with the dual-functions SPIONs.

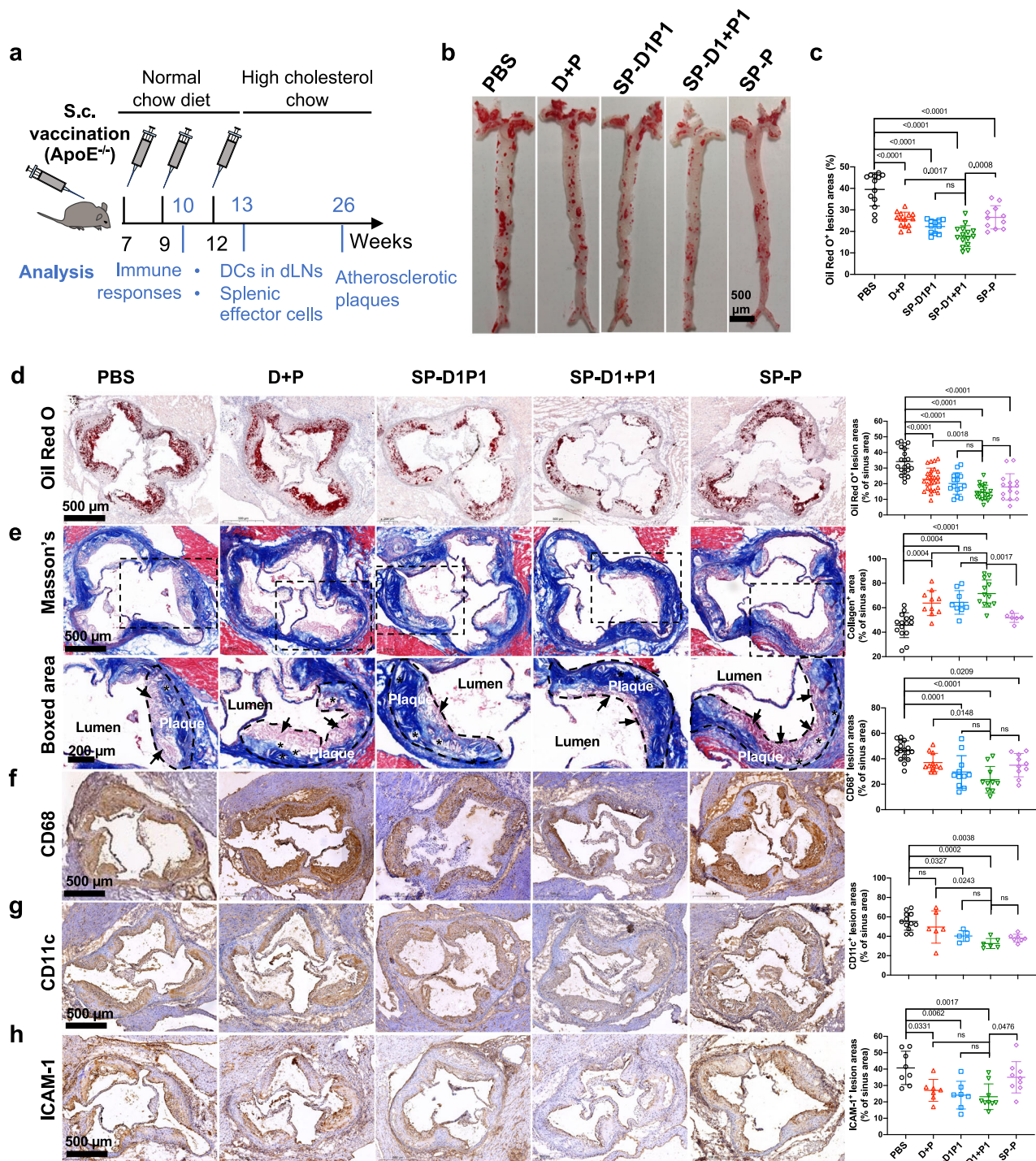


Fig. 7 | SPION-based nanovaccines reduce and stabilize atherosclerotic plaques. **a** Schedule for full vaccination of ApoE^{-/-} mice and analysis timeline. One week after the final booster, mice were switched to a high-cholesterol diet that continued until euthanasia at the age of 26 weeks. **b** Representative images of Oil Red O-stained aortas of ApoE^{-/-} mice; Oil Red O stains fat (red). **c** Fractional plaque areas in total aorta for mice given SP-D1 + P1 ($n = 15$), SP-D1P1 ($n = 11$), D + P ($n = 14$), SP-P ($n = 11$), and PBS ($n = 13$). The data are from biological replicates across 2 batches of experiments and presented as mean \pm SD. Statistical significance was calculated via one-way ANOVA with Tukey's post hoc test. Statistically significant p values are reported; ns means no significance. **d** Representative images of Oil Red O-stained sections of aortic roots and plaque areas in aortic roots for mice given PBS ($n = 21$), D + P ($n = 26$), SP-D1P1 ($n = 15$), SP-D1 + P1 ($n = 19$), and SP-P ($n = 15$). **e** Representative images of Masson's staining of aortic root sections and stained areas in mice given

PBS ($n = 15$), D + P ($n = 10$), SP-D1P1 ($n = 9$), SP-D1 + P1 ($n = 12$), and SP-P ($n = 6$). In the enlarged black boxed areas, the borders of plaques were indicated by black dotted lines, fibrous caps by the black arrows, and necrotic cores by the black asterisks. **f–h** Representative images after immunohistochemistry staining (brown) of the aortic root sections with anti-CD68 antibody (**f**) ($n = 18, 11, 11, 10$, and 10 for PBS, D + P, SP-D1P1, SP-D1 + P1, and SP-P, respectively), anti-CD11c antibody (**g**) ($n = 12, 6, 5, 6$, and 7 for PBS, D + P, SP-D1P1, SP-D1 + P1, and SP-P, respectively), and anti-ICAM-1 antibody (**h**) ($n = 8, 7, 7, 9$, and 9 for PBS, D + P, SP-D1P1, SP-D1 + P1, and SP-P, respectively). The slides were counterstained with hematoxylin (blue) to visualize the cell nuclei. All data are from biological replicates and presented as means \pm SD. Statistical significance was calculated by one-way ANOVA with Tukey's test for *post hoc* analysis. Statistically significant p values are reported; ns means no significance. Source data are provided as a Source Data file.

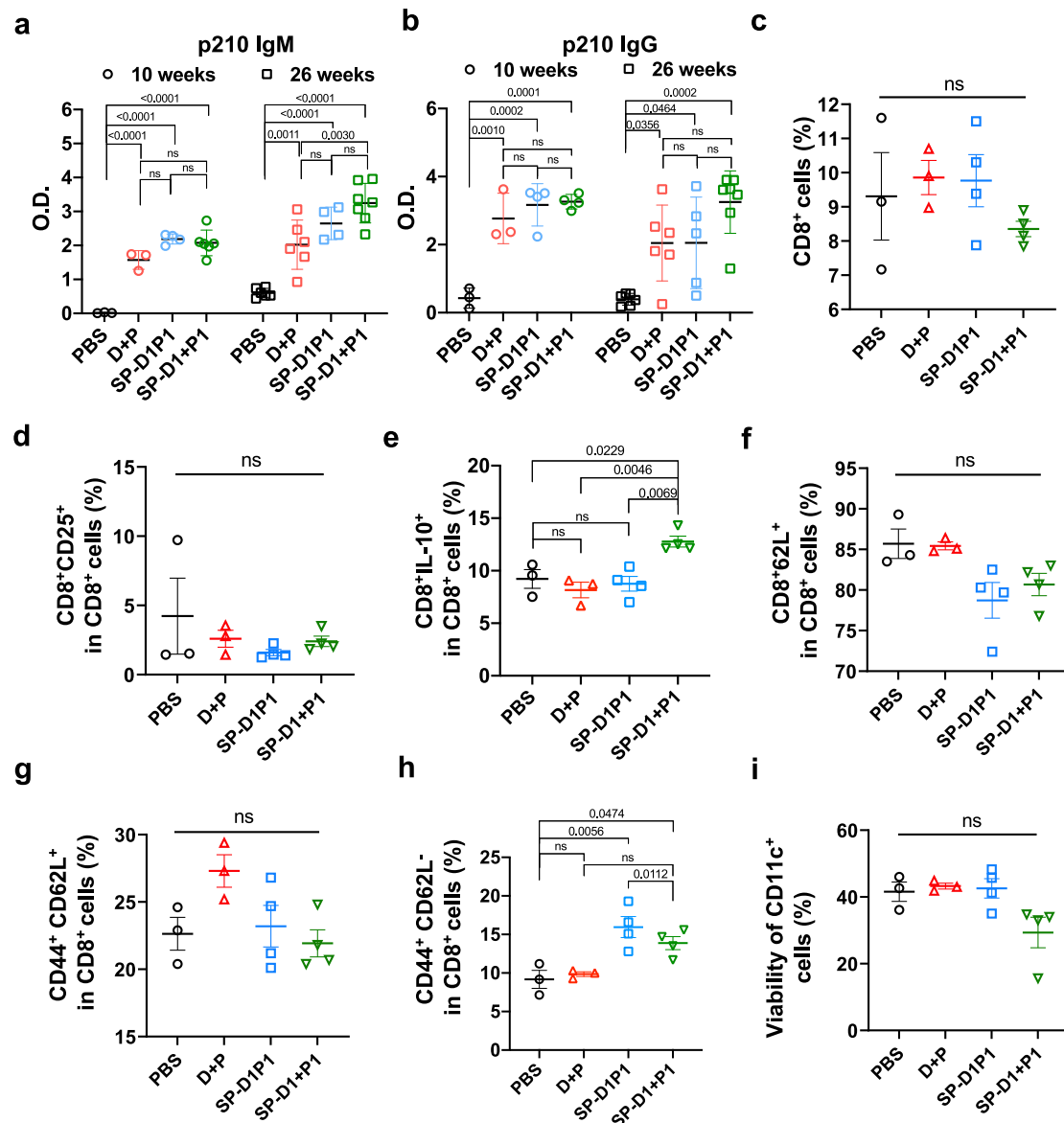


Fig. 8 | Nanovaccines induce humoral responses and CD8⁺ T lymphocyte responses in ApoE^{-/-} mice. Levels of anti-p210 IgM (a) and IgG (b) antibodies levels at 10 weeks and 26 weeks in ApoE^{-/-} mice treated as indicated. $n = 3, 3, 4$, and 6 (10 weeks) and $n = 6, 6, 4$, and 7 (26 weeks) for PBS, D + P, SP-D1P1, and SP-D1 + P1, respectively, for IgM measurement. $n = 3, 3, 4$, and 4 (10 weeks) and $n = 6, 6, 5$, and 7 (26 weeks) for PBS, D + P, SP-D1P1, and SP-D1 + P1, respectively, for IgG measurement. All data are shown as mean \pm SD. Statistical significance was calculated by one-way ANOVA with Tukey's test for post hoc analysis. Statistically significant p values are reported. Flow cytometric analyses of spleen T lymphocytes of ApoE^{-/-}

mice treated as indicated for percentages of CD8⁺ T cells (c), CD8⁺CD25⁺ T cells (d), CD8⁺IL-10⁺ T cells (e), CD8⁺CD62L⁺ T cells (f), CD8⁺ central memory T cells (CD8⁺CD44⁺CD62L⁺) (g), and CD8⁺ effector memory T cells (CD8⁺CD44⁺CD62L⁻) (h). i Viability of BMDc cells cultured for 4 h with CD8⁺ T cells from indicated experimental groups. $n = 3, 3, 4$, and 4 for PBS, D + P, SP-D1P1, and SP-D1 + P1, respectively. All the results are shown as mean \pm SD. Statistical significance between each treatment was calculated by one-way ANOVA with Tukey's test for post hoc analysis. Statistically significant p values are reported; ns means no significance. Source data are provided as a Source Data file.

Next, we tested the cytolytic activities of CD8⁺ T isolated from vaccinated mice against DCs. A week after the second booster (week 13), CD8⁺ T cells were extracted from spleens of vaccinated and control mice and were co-cultured with BMDc that had been cultured in fetal bovine serum-containing culture medium for 10 days. The fetal bovine serum contains ApoB-100 in the low-density lipoprotein cholesterol fraction, so the antigen-experienced BMDc are targets of CD8⁺ effector T cells. Viabilities of the BMDc after incubation with CD8⁺ T cells were assessed by flow cytometry (Supplementary Fig. 27). We found that CD8⁺ T cells from SP-D1 + P1 treated mice had higher cytolytic activity (~29% of BMDc survived) than CD8⁺ T cells from mice vaccinated with other preparations or with PBS (~42% of BMDc survived; Fig. 8i).

Although a high-cholesterol diet enhances the systemic proinflammatory response and activation of T cells, anticipated to occur along with the enlargement of lymph nodes draining the atherosclerotic aorta⁶¹, the CD11c⁺ cell fraction in the draining lymph nodes of ApoE^{-/-} mice was significantly decreased at week 26 by vaccination with SP-D1 + P1 group (Supplementary Fig. 28a). Although no obvious differences were detected in the CD8⁺CD25⁺ T cell population (Supplementary Fig. 28b), the total CD8⁺ T cell population decreased in the vaccinated groups compared to the PBS-treated mice (Supplementary Fig. 28c). The percentage of splenic CD8⁺CD62L⁺ cells, CD8⁺ central memory T cells, and CD8⁺ effector memory T cell populations at 26 weeks were not significantly different in vaccinated and control mice (Supplementary Fig. 28d-f). T cell activation is a hallmark of

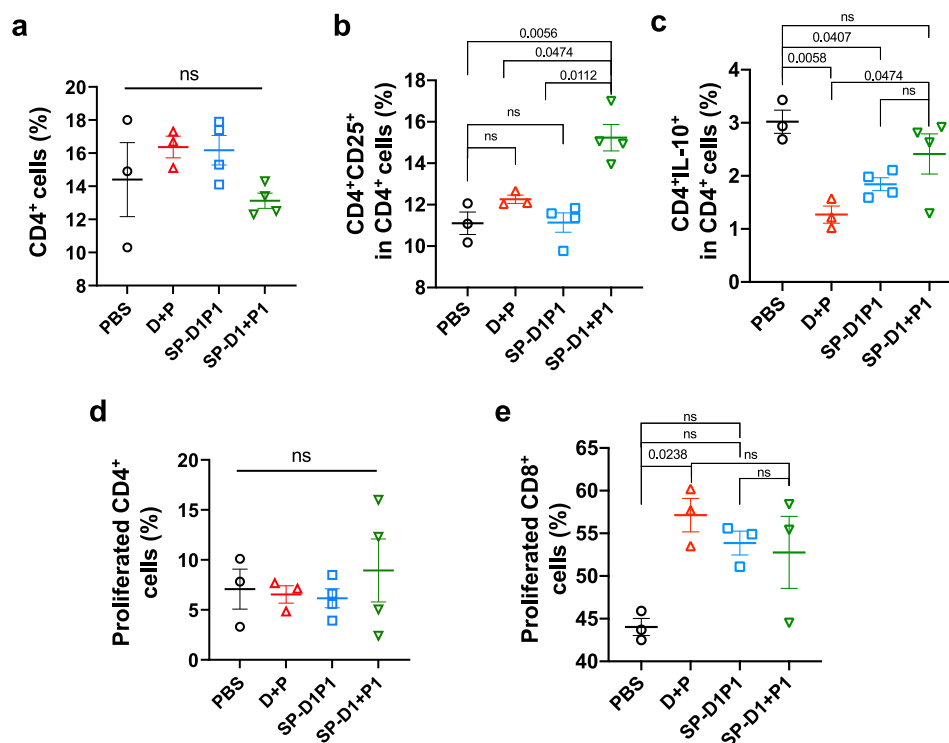


Fig. 9 | Nanovaccines induce CD4⁺ T lymphocyte responses in $ApoE^{-/-}$ mice.

Flow cytometric analyses of spleen T lymphocytes from $ApoE^{-/-}$ mice at 10 weeks post vaccination for percentages of CD4⁺ T cells (a), CD4⁺CD25⁺ T cells (b), CD4⁺IL-10⁺ T cells (c). $n = 3, 3, 4$, and 4 for PBS, D + P, SP-D1P1, and SP-D1 + P1, respectively. Spleen T lymphocytes isolated from C57BL/6 mice at week 15 post-vaccination were labeled with CFSE and stimulated with p210 for 5 days and CD4⁺ ($n = 3, 3, 4$, and 4

for PBS, D + P, SP-D1P1, and SP-D1 + P1, respectively) (d) and CD8⁺ ($n = 3$ animals per group) (e) T cell proliferation was quantified. The data are shown as mean \pm SD. Statistical significance was calculated by one-way ANOVA with Tukey's test for *post hoc* analysis. Statistically significant *p* values are reported; ns means no significance. Source data are provided as a Source Data file.

atherosclerosis in $ApoE^{-/-}$ mice fed a high-cholesterol diet⁶². For example, the T helper cells mature into antigen-experienced effector memory and central memory cells^{63,64} that might mask the immunological responses brought about by the nanovaccines. Therefore, we found that nanovaccinations (especially SP-D1 + P1) elicited CD8⁺ T cell response by increasing the CD8⁺IL-10⁺ population, CD8⁺ effector memory cells, and cytotoxic activity to dendritic cells at one week after the primary booster, but not to an obvious extent at a later stage of atherosclerosis.

We also analyzed the CD4⁺ T subpopulations in the spleens of immunized $ApoE^{-/-}$ mice at week 10. No differences in the percentages of total CD4⁺ T cells (Fig. 9a) were observed, but a significant increase was detected in CD4⁺CD25⁺ regulatory T cells in the SP-D1 + P1-treated group compared to the control mice (Fig. 9b); an increase in this population was previously associated with the reduction of atherosclerosis^{12,65}. In addition, vaccinations with SP-D1 + P1, SP-D1P1, and D + P decreased the percentage of CD4⁺IL-10⁺ T cell population compared to PBS-treated control group, with SP-D1 + P1 resulting in the highest increase (Fig. 9c). These data suggest that SP-D1 + P1 elicits both CD8⁺ and CD4⁺ T cell responses. How these cells mediate the atheroprotective effect is debated^{54,66}. Populations of splenic CD4⁺CD62L⁺ cells, CD4⁺ effector memory T cells (CD4⁺CD44⁺CD62L⁺), and CD4⁺ central memory T cells (CD4⁺CD44⁺CD62L⁺) were not altered at week 10 or at week 26 by vaccination (Supplementary Fig. 29).

We next performed experiments in wild-type mice to minimize the effect of confounding factors that may arise from the potential antigenic exposure resulting from serum cholesterol. T cell proliferation was assessed by cytometric analysis of splenic cells from immunized C57BL/6 mice at week 15, three weeks after the secondary booster (Supplementary Fig. 30). Stimulation with p210 for 5 days did

not cause appreciable CD4⁺ T cell proliferation (Fig. 9d) but did result in higher average values of CD8⁺ T cell proliferation in vaccinated mice compared to controls (Fig. 9e). As both CD8⁺ T and CD4⁺ T responses were observed in $ApoE^{-/-}$ mice at 10 weeks of age, we also measured the cytokines related to the two T cell subtypes. CD8⁺ T effector cells mainly secrete proinflammatory cytokines like TNF- α and IFN- γ ⁶⁷, whereas regulatory T cells are believed to exert atheroprotection by secreting IL-10⁶⁸. In both $ApoE^{-/-}$ and C57BL/6 mice, we found that the nanovaccinations increased IFN- γ and IL-10 levels and that SP-D1 + P1 was even more potent than SP-D1P1 (Supplementary Fig. 31a–d). This observation, however, did not persist for the long term as we did not find significant differences at 26 weeks in $ApoE^{-/-}$ mice (Supplementary Fig. 31e, f). IFN- γ inhibits IL-10 expression^{69,70}, but it stimulates IL-10 production in B cells triggered with CpG-ODNs that are TLR9 agonists⁷¹. As anti-p210 antibodies are present at 10 weeks in vaccinated $ApoE^{-/-}$ mice, B cells as well as both CD4⁺ and CD8⁺ T cell-mediated immune responses might be involved in the response to atherosclerotic plaques after vaccination with SP-D1P1 and SP-D1 + P1.

Discussion

In this study, we prepared a “cocktail” vaccine against atherosclerosis by conjugating p210 and CpG-ODNs onto separate SPIONs and mixing them at 1:1 ratio (Fig. 10). The SPION-based carrier substantially upregulates the uptake of antigens and adjuvants into DCs via SR-A and MR-mediated endocytosis, respectively. The disassembled endolysosomal localizations of the SP-D and SP-P enhanced the cross-presentation of antigens, maximizing the activation of DCs in a way to promote type 1 immunity. Three subcutaneous doses of SP-D1 + P1 prophylactically mitigated the plaque progression in $ApoE^{-/-}$ mice challenged by a high-cholesterol diet. Our results suggest the MR-mediated uptake of p210

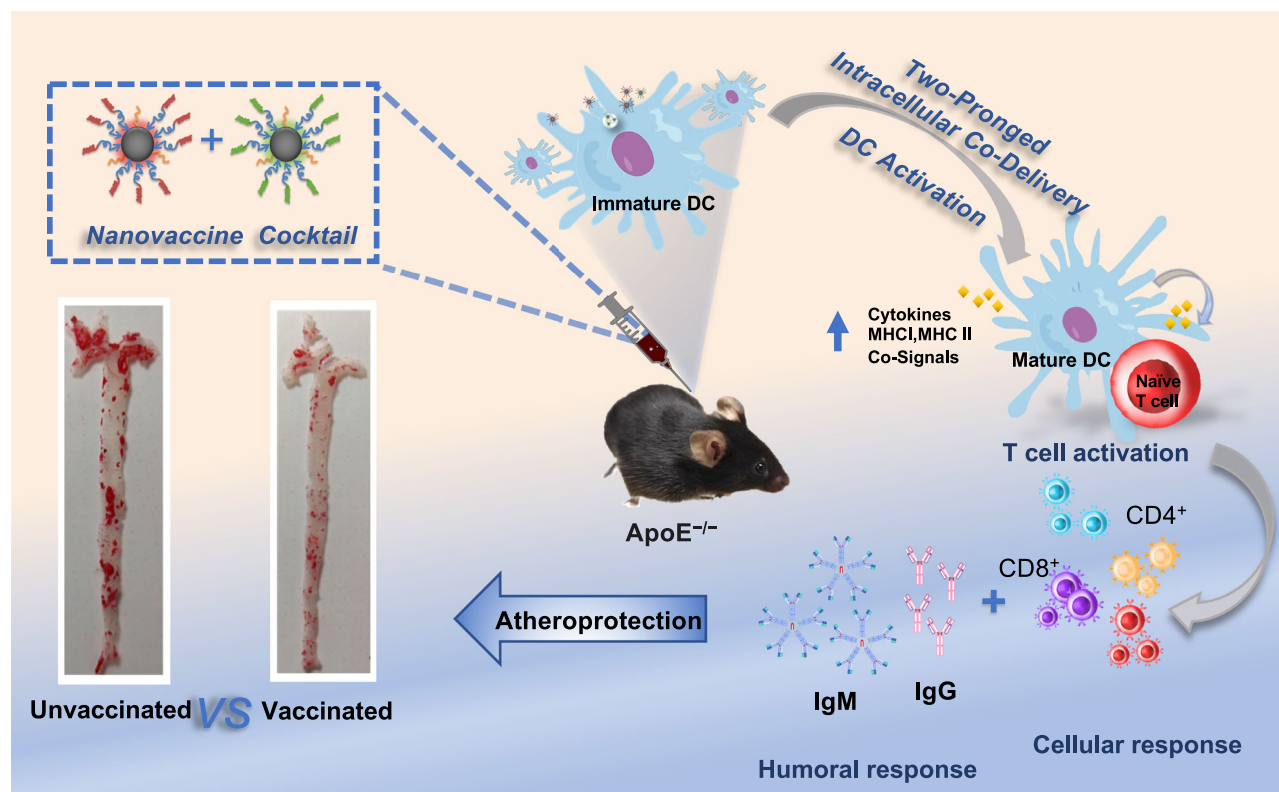


Fig. 10 | Nanovaccine cocktail significantly inhibits atherosclerotic progression by activating both humoral and cellular immune responses. The two-pronged delivery of SP-D and SP-P modulates the DCs in the draining lymph nodes inducing

type 1 cytokine secretion and co-signal expression, generates regulatory and memory responses in both CD4⁺ and CD8⁺ T cells, and induces both anti-p210 IgM and IgG antibodies to achieve an atheroprotective effect.

conjugated to the SPION facilitates antigen routing into the endosomal compartment for better MHC class I presentation, as evidenced by the CD8⁺ T proliferation. In deciphering the working mechanism of nanovaccines, we collected evidence of increased CD8⁺IL-10⁺ and CD4⁺CD25⁺ T cell populations shortly after full vaccination. The cell-mediated immune responses, however, were not obvious at the later stage of atherosclerosis. Humoral responses, on the other hand, might provide longer term of protection, as evidenced by the generation of both anti-p210 IgM and IgG antibodies that lasted for a longer duration of time. How effector cells mediate the atheroprotective process and how long the nanovaccines protect against atherosclerosis require further investigation, but our findings demonstrate that the two-pronged nanovaccine delivery strategy is effective against atherosclerosis.

Methods

Materials

Polyethylene glycol 2000 (OH-PEG₂₀₀₀-OH, Catalog No. 8210371000), potassium bromide (KBr, ≥99.0%, Catalog No. 243418), 2,2,6,6-tetramethyl-1-piperidinyloxy (TEMPO, 98%, Catalog No. 214000), iron (III) acetylacetonate [Fe(acac)₃, ≥99.0%, Catalog No. 517003], and oleylamine (technical grade, 70%, Catalog No. 07805) were purchased from Sigma-Aldrich (US). Sodium hypochlorite solution (HClO, ~8%, Catalog No. S101636), diphenyl ether (≥99.9%, Catalog No. D130016), dichloromethane (DCM, CH₂Cl₂, ACS grade, Catalog No. D433567), *N*-hydroxysuccinimide (NHS, ≥98%, Catalog No. H109330), and *N,N*-dicyclohexylcarbodiimide (DCC, ≥99%, Catalog No. D106074) were purchased from Aladdin Chemicals Co., Ltd (China). Anhydrous diethyl ether (≥99.0%, Catalog No. AH1045B) was purchased from RCI Labscan Group (Thailand). Anhydrous dimethyl sulfoxide (99.8%, Catalog No. 043998) was purchased from Alfa Aesar Fine Chemicals & Metals (Fisher Scientific, US). Ethanol (EtOH, 95%, Catalog No. E801077) were

purchased from Macklin Chemicals Co., Ltd (China). Hydrochloric acid (HCl, 36.0–38.0%, AR grade, Catalog No. 10011018) and sodium hydroxide (NaOH, ≥96%, AR grade, Catalog No. 10019718) were purchased from China National Pharmaceutical Group Co Ltd (Sino-pharm). All the chemicals were used without purification if no further specification was given. The CpG-ODNs with amine functionalization (fully thiol-modified oligodeoxynucleotide CpG 1826, 5'-tcc atgacgttcctgacgtt-NH₂) and Quasar 670-labeled CpG-ODNs at the 5'-end (≥99%) were purchased from Shanghai DNA Bioscience Co. Ltd (Shanghai, China). The p210 peptide (KTTKQ SFDLS VKAQY KKNKH) and p210 labeled with TAMRA or FITC in the N-terminal (≥95%) were ordered from Nanjing Peptide Biotech Ltd (Jiangsu, China).

Synthesis of PEG-SP

Dicarboxyl-terminated PEG (Mw=2000, termed as HOOC-PEG₂₀₀₀-COOH) was prepared by oxidation of HO-PEG₂₀₀₀-OH with TEMPO following previous protocol⁷². Typically, 10 g of HO-PEG₂₀₀₀-OH (10 mmol primary alcohol), 7.8 mg of TEMPO (0.05 mmol), and 0.119 g of KBr (1 mmol) were fully dissolved in 70 mL of deionized water (D.I. water). In a separate beaker, HClO solution (8%, w/v) containing 30 mmol active chlorine was adjusted to pH 10 by adding 4 M HCl solution. Both solutions were mixed after cooling below 4 °C on ice bath, and the temperature of the mixture was maintained below 4 °C while the pH was maintained at pH 10 by addition of 0.5 M NaOH during the 5 h of oxidation reaction. After adding 5 mL of EtOH to quench the reaction, the pH of solution was adjusted to 3 by addition of 4 M HCl. The obtained HOOC-PEG₂₀₀₀-COOH was extracted three times with CH₂Cl₂, concentrated by rotary evaporator, precipitated with diethyl ether, crystallized from EtOH, and stored at -80 °C for future use.

SPIONs coated with HOOC-PEG₂₀₀₀-COOH were prepared by thermal decomposition method according to previous study³⁴.

Typically, 525 mg of ferric acetylacetonate [Fe(acac)₃], 6.0 g of HOOC-PEG₂₀₀₀-COOH, and 2.0 mL of oleylamine were added in 25.0 mL of diphenyl ether. After aging the mixture at 80 °C under nitrogen for 4 h, the reaction was heated to 260 °C at a rate of 10 °C/min and kept at reflux for 30 min. By re-dispersing the product in ethanol and precipitating with chilled diethyl ether for three cycles, the obtained PEG-SPs were purified, dialyzed against deionized water for 48 h, filtered via 0.22 µm syringe filter, and freeze-dried. The lyophilized particles were tightly sealed and stored at −80 °C until used.

Preparation of SPION-based nanovaccines

Typically, 10 mg of PEG-SPIONs were dissolved in 1 mL of anhydrous DMSO, activated with 40 µmol of DCC and 60 µmol of NHS for 2 h before 12 nmol of CpG-ODN, 12 nmol of p210, or mixture of CpG-ODN and p210 were added (total 12 nmol at a molar ratio of x to y), which yield to SP-D, SP-P, and SP-DxPy, respectively. The mixture was sonicated for 30 min and left on an orbital shaker for 8 h. After dialyzing against distilled water for 48 h, the nanoparticles were filtered with 0.22 µm syringe filter and freeze-dried. SP-Dx+Py was prepared as physical mixture of SP-D and SP-P at a molar ratio of x to y.

Characterizations of PEG-SP and SPION-based nanovaccines

The size and morphology of the PEG-SPs were determined by TECNAI G2 20 transmission electron microscope (TEM) (LaB6, FEI Netherlands). The hydrodynamic sizes and zeta potentials of the nanoparticles were tested in both water and complete cell culture medium using Zetasizer Nano ZS90 (Malvern, UK) with Zetasizer family software (version 8.01). The magnetic property of the lyophilized PEG-SPs was measured by using a vibrating sample magnetometer (VSM, HH-15). Magnetization was measured over a range of applied field from −6000 Oe to 6000 Oe at 300 K. The thermogravimetric analyses (TGA) of the dried samples were performed using a thermogravimetric analyzer (SDTA 851e, Mettler Toledo, Switzerland) at a heating rate of 10 °C/min from room temperature to 600 °C under nitrogen flow. The surface coating of the nanoparticles was recognized by Fourier transform infrared spectroscopy (Nicolet iS20, Thermo Fisher, USA) ranging from 500 cm^{−1} to 4000 cm^{−1} with a step size of 4 cm^{−1}. The gel electrophoresis of nanoparticles was performed in 0.5% agarose gel soaked in 1% TAE buffer at 120 V for 20 mins.

Culture of BMDCs

Monocytes were isolated from the femurs and tibias of C57BL/6 mice at age of 4–6 weeks and differentiated to BMDCs according to previous protocol⁷³. Specifically, mice kept under specific pathogen-free conditions were euthanized by CO₂ inhalation followed by cervical dislocation. After removing the femurs and tibiae, they were rubbed with Kleenex tissues to remove the surrounding muscle tissues. After soaking the intact bones in 70% ethanol for 3 min, they were washed with PBS, cut open at both ends. The bone marrow was flushed with cold PBS using a syringe with a 22-gauge spinal needle, passed through the 70 µm cell strainer, and collected with a sterilized 50 mL conical tube. The leukocytes were pelleted by centrifugation at 500 g for 5 min and suspended in cell culture medium. Cells were cultured at a density of 10⁶/mL in DC culture medium composed of RPMI medium (Thermo Fisher Scientific) supplemented with 10% FBS (Gibco, Thermo Fisher Scientific, Catalog No. A5256701), 10 units/mL penicillin and 10 µg/mL streptomycin (Gibco, Thermo Fisher Scientific, Catalog No. 15070063), 50 µM β-mercaptoethanol (β-ME) (Gibco, Thermo Fisher Scientific, Catalog No. 21985023), 2 mM L-glutamine (Gibco, Thermo Fisher Scientific, Catalog No. A2916801), 20 ng/mL murine GM-CSF (Novoprotein Technology, China, Catalog No. CK02) and 10 ng/mL murine IL-4 (Novoprotein Technology, China, Catalog No. CK15) at 37 °C and 5% CO₂. Fresh medium containing the same concentration of growth factors was added to cells on Day 3 and Day 7. On Day 8, the cells were ready to use.

Animals

Male ApoE knockout (ApoE^{−/−}) mice aged 4–5 weeks (stock No. T001458) and age-matched male C57BL/6JGpt mice (stock No. N000013) were provided by Gem Pharmatech Company, China. The animals were housed in a specific pathogen-free animal facility accredited by Nanjing First Hospital, Jiangsu, China. The mice were kept on a 12 h day/night cycle at temperature of 20–26 °C and relative humidity of 40–70% with unrestricted access to water and food. Experimental/control mice from each litter were co-housed in individually vented cages on the same rack in the animal facility. All animal procedures followed the guidelines stipulated by the Animal Experimentation Ethics Committee (AEEC) at Nanjing First Hospital, Jiangsu, China (DWSY-1901323).

Cell proliferation study

BMDCs were seeded in a 96-well plate at a density of 5.0 × 10⁵ cells per well in 200 µL complete DC culture medium for 24 h at 37 °C. The SPION-based vaccines were added at different concentrations (0–1000 µg/mL) to the BMDCs and incubated for 24 h before the Cell Counting Kit-8 (CCK-8) (Apexbio, USA, Catalog No. K1018) was performed according to the manufacturer's protocol.

Cell uptake, pharmacological inhibition, and intracellular trafficking

The nanovaccines made from Quasar 670-labeled CpG-ODN and FITC-tagged p210 were added to the BMDCs pre-seeded on 12 mm glass coverslips (Marienfeld, Fisher Scientific, Catalog No. 10006111) in 24-well plates and incubated for different durations of time. The cells were then fixed with 4% paraformaldehyde (PFA) (Beyotime, China, Catalog No. P0099), washed with PBS three times, stained with Hoechst 33342 (Beyotime, China, Catalog No. C1022) and mounted with Fluoromount-G mounting medium (Absin, China, Catalog No. abs9240).

For pharmacological inhibition study, BMDCs were pre-treated with cell culture medium containing different concentrations of chemical blockers or blocking antibodies for 1 h. These blockers include fucoidan (50 µg/mL, Yuanye Bio-Technology, China, Catalog No. S11142), mannan (1 mg/mL, Yuanye Bio-Technology, China, Catalog No. S51698), amiloride (500 µg/mL, Glpbio, USA, Catalog No. GC17853), antibody against CD16/32 (10 µg/mL, BioLegend; 101302). After removing the inhibitor-containing medium, 0.3 mL of serum-containing cell culture medium that contains the same inhibitor at the original concentration and 200 µg/mL of SP-P, SP-D, SP-D1P1, and SP-D1 + P1 were subsequently added to the cells. After 4 h of incubation, the medium was removed, and the cells were rinsed with PBS. The cells were then fixed with 4% PFA, washed with PBS three times, stained with Hoechst 33342, and mounted with Fluoromount-G mounting medium.

In the intracellular trafficking of nanovaccines, the cells were incubated with fluorescently tagged nanovaccines for different durations of time. The cells were washed with PBS and stained with Lyso-Tracker Red (Beyotime, China, Catalog No. C1046) alive according to the manufacturer's protocol.

In the three studies above, the cells were prepared to be visualized by using an Olympus confocal microscope (FV3000) with FV31S-SW Viewer software (version 2.3.1). The excitation wavelength for Hoechst 33342/DAPI was 405 nm, and the corresponding emission filter was 440–500 nm. The excitation wavelength for the FITC-labeled nanovaccines was 488 nm, and the corresponding emission filter was 500–530 nm. The excitation wavelength for Quasar 670-labeled nanovaccines was 640 nm, and the corresponding emission filter was 650–750 nm. ImageJ (Fiji contributors) with a JACoP plugin (version 1.53) was used to quantify the colocalization of the two fluorescence signals in the images required, and the Pearson's colocalization coefficient was calculated. The average fluorescence intensities of the

nanovaccines before and after pharmacological treatments were also measured by Fiji.

BMDCs in vitro activation

BMDCs were seeded in a 24-well plate at a density of 1.0×10^6 cells per well in 1 mL of complete RPMI medium for 24 h at 37 °C. Next, the cells were treated with various SPION-based vaccines (300 µg/mL), physical mixture of CpG-ODN and p210 (500 nM each), and the counterparts without nanoparticle conjugation (500 nM for CpG-ODN and p210) for 24 h or 72 h. Lipopolysaccharides (LPS) from *Escherichia coli* (Beyotime, China, Catalog No. ST1470) were added at 1 µg/mL as positive controls. The cells were then collected with cold PBS treatment for flow cytometric analysis or quantification of Fe content by inductively coupled plasma mass spectrometry (ICP-MS).

To check the surface expression of different markers, the collected cells were stained with Fc blocker (anti-mouse CD16/32) together with APC anti-mouse CD11c, FITC anti-mouse CD40, FITC CD80 (B7-1) monoclonal antibody, PE anti-mouse CD86, PE MHC Class I (H-2Kb) monoclonal antibody, or FITC MHC Class II (I-A/I-E) monoclonal antibody before staining with Zombie Aqua fixable viability dye (BioLegend; 423101). Finally, the cells were resuspended in 200 µL FACS buffer (5 mM EDTA and 1% FBS in PBS) for flow cytometry analysis. The antibodies used for flow cytometric analysis including the clone, type, supplier, catalog number, and dilution are summarized in Supplementary Table 1. To quantify the cellular uptake of Fe in each treatment, the cells from each well were digested with 65% HNO₃ for 12 h, diluted with deionized water to 2% HNO₃ solution, and analyzed with ICP-MS (iCAP Q, Thermo Fisher, USA).

For cytokine expression, the cells were incubated with SPION-based vaccines (300 µg/mL) or the counterparts without nanoparticle conjugation (500 nM for CpG-ODN and p210; 1 µg/mL for LPS) for 24 h. The supernatants were collected and the cytokine levels (TNF-α, IL-6, and IL-12p70) were tested with individual enzyme-linked immunoassay (ELISA) kits according to the manufacturer's protocol (Multisciences Biotech, China, Catalog No. EK282, EK206, and EK212, respectively).

T cell priming in vitro

The male C57BL/6 mice aged at 4–5 weeks were euthanized by CO₂ inhalation followed by cervical dislocation before collecting the spleens and bone marrow monocytes. The splenocytes in single cell suspensions were cryopreserved after lysis of red blood cells, and the monocytes were cultured into BMDCs as indicated above. BMDCs were activated by addition of SPION-based vaccines (300 µg/mL) or D + P (500 nM CpG-ODN and p210) for 24 h, and the autologous splenocytes were labeled by carboxyfluorescein succinimidyl ester (CFSE) (Thermo Fisher Scientific; C34554) and cocultured with BMDCs for 4 days for T cell priming. The supernatants after co-culture were collected and tested for the cytokine levels including INF-γ, IL-10, IL-12, and IL-17 according to the manufacturer's protocol (Multisciences Biotech, China, Catalog No. EK280, EK210, EK212 and EK217). The cells were then collected with cold PBS treatment for flow cytometric analysis. Cells were stained with Fc blocker (anti-mouse CD16/32,) together with BV786 CD3e monoclonal antibody, FITC anti-mouse CD4 antibody, PE-eFluor 610 CD8a monoclonal antibody, eFluor 450 CD62L monoclonal antibody, PE-Cyanine5 CD44 monoclonal antibody. The cells were then stained with Zombie Aqua Fixable Viability Kit (BioLegend; 423101) and resuspended in 200 µL of FACS buffer for flow cytometry analysis by a BD FACSCeleste cell analyzer. Data were analyzed by the FCS Express 7 software (Reachsoft) (Version 7.18.0030).

dLN trafficking of nanovaccines in vivo

The male C57BL/6 mice aged at 6–7 weeks were subcutaneously injected with different vaccines into the dorsal area between the scapulas. At different timepoints (20 h, 48 h, and 72 h) after injection, the mice were euthanized by CO₂ inhalation followed by cervical

dislocation, and both brachial and inguinal lymph nodes were collected. The samples were photoed by a Xiaomi cell phone, fixed with 10% formalin solution (Solarbio Life Sciences, China, Catalog No. G2162) embedded in paraffin, and sectioned into 10 µm-thick slides. Paraffin-sections were deparaffinized in xylene, rehydrated through a series of ethanol (100%, 90%, 70%), and deionized water. The sections were further subjected to immunohistochemistry staining of CD11c (1:400 dilution, Servicebio; GB11059), CD68 (1:400 dilution, Servicebio; GB113109), or CD3 (1:1000 dilution, Servicebio; GB150004), and Prussian blue staining (Servicebio; GP1068) to visualize the localization of SPIONs.

In another experiment, the mice were subcutaneously injected with different vaccines ($n = 3$), in which the CpG-ODNs were labeled with Quasar 670 at the 5'-end, and p210 were labeled with FITC in the N-terminal. At 20 h after injection, the mice were euthanized as above. The dLNs were extracted and passed through a 70 µm cell strainer, stained with Fc blocker (anti-mouse CD16/32) together with and PE anti-mouse CD86. The cells were then stained with Zombie Aqua Fixable Viability Kit (BioLegend; 423101) and resuspended in 200 µL of FACS buffer for flow cytometry analysis by a flow cytometer (BD FACSCantoll). Data were analyzed by the FlowJo 10 software (Tree Star).

Biodistribution of nanovaccines in vivo

The male C57BL/6 mice aged at 6–7 weeks were shaved in the back, subcutaneously injected with different vaccines into the scruff area of the necks ($n = 3$), in which the nanovaccines were formulated with Quasar 670 labeled CpG-ODNs and TAMRA-labeled p210. After injection, the mice were subjected to in vivo fluorescence imaging by the VISQU® InVivo Smart-LF system (Viewworks, Korea) at 4 h to 7 days (168 h). A separate group of mice was first fully anesthetized at 20 h post injection by the RWD isoflurane anesthesia system (RWD Life Science, China) and retro-orbital blood was collected for serum separation. After euthanasia by cervical dislocation, the dLNs near the injection sites and major internal organs were collected for fluorescence imaging by the in vivo imaging system. The dLNs were then fixed by 10% formalin, embedded with paraffin, and sectioned for 10 µm-thick slides for immunofluorescence staining. They were first stained with primary antibodies including CD11c (1:400 dilution, Servicebio; GB11059) and CD68 (1:400 dilution, Servicebio; GB113109), further stained with secondary antibody FITC-conjugated goat anti-rabbit IgG (H + L) (1:200 dilution, Servicebio; GB22303), washed, and stained with Hoechst 33342 and mounted with Fluoromount-G mounting medium. Samples were imaged by a panoramic scan II digital scanner (3Dhistech, Hungary) provide by Nanjing Youmeng Biotechnology Co., Ltd. (China) and processed by the SlideViewer Software (Version 2.1.76).

Immunization protocol

Male ApoE^{-/-} aged 4–5 weeks mice were first maintained on normal chow diet (Cat. No. 1010001, Jiangsu Xietong Pharmaceutical Bio-engineering Co., Ltd., China), each received subcutaneous primary immunization of PBS, mixture of 20 nmol of CpG-ODN and 20 nmol of p210 (D + P), 2.5 mg of SP-DIP1 (containing -3.0 nmol of CpG-ODN and 3.2 nmol of p210), or 2.5 mg of SP-D1 + P1 (containing -2.2 nmol of CpG-ODN and -3.7 nmol of p210) in the dorsal area between scapula at 7 weeks of age, followed by a booster at 9 and 12 weeks of age. One week after the last booster, the diet was switched to high cholesterol chow (Cat. No. XT108C, Jiangsu Xietong Pharmaceutical Bio-engineering Co., Ltd., China) and continued until euthanasia at the age of 26 weeks. The mice were first fully anesthetized by isoflurane inhalation for retro-orbital blood collection and euthanized by cervical dislocation, followed by organ collection. Other mice under the same immunization protocol (both male ApoE^{-/-} and age-matched C57BL/6 mice) were treated by the same procedures one week after the primary booster injection to access immune responses by flow cytometry.

Harvesting, preparation, and staining of aorta and aortic roots
 ApoE^{-/-} mice were euthanized and the whole aortas were harvested, washed with PBS, and stained with Oil Red O (ORO) staining solution (Sigma-Aldrich) to assess the development of atherosclerosis en face. The samples were imaged, and the percentage of ORO-positive area was calculated by ImageJ software (version 1.53). The hearts were harvested and embedded in OCT compound (Sakura Finetek, USA), froze at -80 °C, and serially sectioned into 10 µm-thick slices. After fixation, cryosections were blocked with 2% bovine serum albumin (BSA) for 1 h, and stained with PBS containing 2% BSA and primary antibodies for 1 h at room temperature. The primary antibodies include recombinant rabbit primary antibody against CD68 (1:200 dilution, Servicebio; GB113109), rabbit polyclonal primary antibody against ICAM-1 (1:50 dilution, Proteintech; 10020-1-AP), and anti-CD11c rabbit primary antibody (1:400 dilution, Servicebio; GB11059). The aortic sections were further stained with HRP-conjugated goat anti-rabbit IgG(H+L) (1:1000 dilution, Servicebio; G1213) and developed over a 3,3'-diaminobenzidine (DAB) solution (Servicebio; G1212). Samples were then mounted and imaged by the panoramic scan II digital scanner (3Dhistech, Hungary) and processed by the SlideViewer Software (Version 2.1.76).

Serum ELISA, liver function, and cholesterol level analysis

ELISA basic kit (Multisciences; 70-EK0011) was used to prepare the p210 pre-coated 96 well plates for detection of anti-p210 IgM and IgG in the mice serum. Specifically, 20 µg/mL of p210 was added to the plates and incubated at 4 °C overnight to assess antibody levels according to the manufacturer's protocol. HRP-conjugated goat anti-mouse IgG Fc (Abcam; ab97265) or IgM µ chain specific (Proteintech; SA00012-6) was used as detecting antibodies, which was further detected by developing in TMB (Multisciences Biotech, Catalog No. 70-E0231) as substrate. The optical density values were recorded at 450 nm, using 570 nm as the reference by a Tecan multimode microplate reader (Infinite F50, Tecan group Ltd., Switzerland). The other cytokine levels in the serum including IFN-γ and IL-10 were tested with ELISA kits according to the manufacturer's protocol (Multisciences Biotech, Catalog No. EK280 and EK210).

The liver functions after vaccination were assessed by measuring levels of serum albumin (ALB), aspartate aminotransferase (AST), and alanine transaminase (ALT) in the C57BL/6 mice at 20 h post the first injection, or 1 week after the third injection of vaccines (week 13), respectively. The plasma cholesterol levels including total cholesterol (TC), high-density lipoprotein cholesterol (HDL-C), low-density lipoprotein cholesterol (LDL-C), and triglycerides (TG) were measured in the immunized ApoE^{-/-} mice at the age of 26 weeks. All the measurements were performed with the commercially available kits from Rayto Life and Analytical Sciences Co., Ltd according to the manufacturer's protocol.

Flow cytometry for immune regulatory profile in vivo

At 10 weeks and 26 weeks of age, the immunized ApoE^{-/-} mice were anesthetized for blood collection and euthanized as indicated above. The spleens and dLNs were excised, minced, and filtered (70 µm; BD Biosciences) to generate a single-cell suspension and centrifuged at 4 °C at 1800 rpm for 10 min. After lysis of red blood cells, the pelleted splenocytes were resuspended in FACS buffer together with APC anti-mouse CD11c antibody, PE CD4 monoclonal antibody, PE CD8a monoclonal antibody (53-6.7), APC anti-mouse CD25 antibody, FITC IL-10 monoclonal antibody, APC anti-mouse CD62L antibody, and FITC anti-mouse/human CD44 antibody. The dLNs were extracted and passed through a 70 µm cell strainer, stained with Fc blocker (anti-mouse CD16/32) together with APC anti-mouse CD11c antibody and PE anti-mouse CD86. The cells were then stained with Zombie Aqua Fixable Viability Kit (BioLegend; 423101) and resuspended in 200 µL of FACS buffer for flow cytometry analysis by a flow

cytometer (BD FACSCantoll). Data were analyzed by the FlowJo software (Tree Star).

CD8⁺ T cell isolation from animals and co-culture with BMDCs

Immunized ApoE^{-/-} mice at the age of 13 weeks were euthanized by CO₂ inhalation followed cervical dislocation and the splenocytes were collected as above. The CD8⁺ T cells were then isolated using BD IMag cell separation kit (anti-mouse CD8a particles-DM 53-6.7, BD Pharmingen; 551516) per manufacturer's protocol, and co-cultured with BMDCs in a CD8: DC ratio of 3:1. After co-culture for 4 h, the cells were collected and processed for flow cytometric determination of CD11c and live/dead staining by the Zombie Aqua Fixable Viability Kit (BioLegend; 423101).

T cell proliferation assay of vaccinated animals in vitro

Male wild-type mice (C57BL/6) were fed on regular chow diet and immunized at the same timepoints as the ApoE^{-/-} mice above. At 15 weeks of age (3 weeks after the second booster), the mice were anesthetized for blood collection and euthanized as indicated above. The splenocytes from each mouse in the treatment group (n ≥ 3) were labeled with 2 µM of CFSE at 37 °C (Thermo Fisher Scientific; C34554) for 10 min. Equal number of cells were seeded into the 6-well plates and stimulated with p210 at 20 µg/mL in complete RPMI medium supplemented with IL-2 at 20 ng/mL (Novoprotein, China, Catalog No. CK24). Cells were harvested after 5 days and stained with PE CD4 monoclonal antibody or PE CD8a monoclonal antibody (53-6.7) and subjected to flow cytometry.

Histological staining for in vivo toxicity

The lower heart, brain, liver, spleen, lung, kidney, and skin around the injection sites were fixed in 10% formalin fixative overnight, embedded in paraffin, and cut into sections of 5 µm thick. Paraffin-sections were deparaffinized in xylene, rehydrated through a series of ethanol (100%, 90%, 70%) and deionized water, and stained by hematoxylin (Sigma-Aldrich, Catalog No. 65066-M) and eosin solutions (Sigma-Aldrich, Catalog No. R03040) (H&E stain). The stained sections were dehydrated in ethanol, cleared in xylene, mounted with Canada balsam mountant (Solarbio Life Sciences, China), and imaged with an inverted fluorescence microscope (Optika, Italy) in bright-field mode. To examine the residual SPIONs in the mouse tissues, the collected organs were also stained with freshly made Prussian blue staining solutions (mixture of 20% hydrochloride and 10% potassium ferrocyanide), counter-stained with Nuclear Fast Red staining solution (Beyotime Biotechnology, China, Catalog No. C0151).

In vivo organ-level distribution of SPIONs

C57BL/6 mice euthanized at 20 h after the first injection of nano-vaccines or ApoE^{-/-} mice at the age of 26 weeks after full vaccination were perfused with saline to remove the blood from the organs as much as possible. The internal organs including were excised and weighted, including heart, lung, liver, spleen, pancreas, kidney, brain, and skin near the injection site. The organs were then each digested in 0.5 mL HNO₃ for three days to ensure full reaction. The lysates were diluted to 2% HNO₃ solution with deionized water and passed through 0.22 µm hydrophilic syringe filters for transparent solutions. The Fe contents were then measured by an iCAP Pro inductively coupled plasma optical emission spectrometer (Thermo Fisher Scientific, USA).

Data processing and statistical analysis

OriginPro software (version 2016 SR0 226) was used for plotting the FTIR, TGA, and VSM results. The GraphPad Prism software (version 10.2.0) was used for data analysis and graph construction. To determine the statistical significance in the comparison of two groups, an unpaired two-tail t test was performed. To determine the statistical

significance in the comparison of multiple groups, an unpaired one-way analysis of variance (ANOVA) was performed with Tukey's test or Dunnett's test for *post hoc* analysis. Results are considered significant at $p < 0.05$.

Reporting summary

Further information on research design is available in the Nature Portfolio Reporting Summary linked to this article.

Data availability

All data are included in the Supplementary Information or available from the authors, as are unique reagents used in this Article. The raw numbers for charts and graphs are available in the Source Data file whenever possible. Source data are provided with this paper. The raw data for flow cytometric analysis have been deposited in the Dryad database [<https://doi.org/10.5061/dryad.zpc866tk7>]. Source data are provided with this paper.

References

- Ross, R. Atherosclerosis—an inflammatory disease. *N. Engl. J. Med.* **340**, 115–126 (1999).
- Hansson, G. K. & Hermansson, A. The immune system in atherosclerosis. *Nat. Immunol.* **12**, 204–212 (2011).
- Lichtman, A. H., Binder, C. J., Tsimikas, S. & Witztum, J. L. Adaptive immunity in atherogenesis: new insights and therapeutic approaches. *J. Clin. Invest.* **123**, 27–36 (2013).
- Palinski, W., Miller, E. & Witztum, J. L. Immunization of low density lipoprotein (LDL) receptor-deficient rabbits with homologous malondialdehyde-modified LDL reduces atherogenesis. *Proc. Natl Acad. Sci. USA* **92**, 821 (1995).
- Roy, P., Ali, A. J., Kobiyama, K., Ghosheh, Y. & Ley, K. Opportunities for an atherosclerosis vaccine: from mice to humans. *Vaccine* **38**, 4495–4506 (2020).
- Colantonio, L. D. et al. Association of serum lipids and coronary heart disease in contemporary observational studies. *Circulation* **133**, 256–264 (2016).
- Nilsson, J. & Hansson, G. K. Vaccination strategies and immune modulation of atherosclerosis. *Circ. Res.* **126**, 1281–1296 (2020).
- Fredrikson, G. N. et al. Identification of immune responses against aldehyde-modified peptide sequences in ApoB associated with cardiovascular disease. *Arterioscler. Thromb. Vasc. Biol.* **23**, 872–878 (2003).
- Fredrikson, G. N., Björkbacka, H., Söderberg, I., Ljungcrantz, I. & Nilsson, J. Treatment with apo B peptide vaccines inhibits atherosclerosis in human apo B-100 transgenic mice without inducing an increase in peptide-specific antibodies. *J. Intern. Med.* **264**, 563–570 (2008).
- Klingenberg, R. et al. Intranasal immunization with an apolipoprotein B-100 fusion protein induces antigen-specific regulatory T cells and reduces atherosclerosis. *Arterioscler. Thromb. Vasc. Biol.* **30**, 946–952 (2010).
- Chyu, K.-Y. et al. CD8⁺ T cells mediate the athero-protective effect of immunization with an ApoB-100 peptide. *PLoS One* **7**, e30780 (2012).
- Wigren, M. et al. Evidence for a role of regulatory T cells in mediating the atheroprotective effect of apolipoprotein B peptide vaccine. *J. Intern. Med.* **269**, 546–556 (2011).
- Fredrikson, G. N. et al. Inhibition of atherosclerosis in ApoE-null mice by immunization with ApoB-100 peptide sequences. *Arterioscler. Thromb. Vasc. Biol.* **23**, 879–884 (2003).
- Gheibi Hayat, S. M. & Darroudi, M. Nanovaccine: A novel approach in immunization. *J. Cell. Physiol.* **234**, 12530–12536 (2019).
- Wang, S. et al. Rational vaccinology with spherical nucleic acids. *Proc. Natl Acad. Sci. USA* **116**, 10473 (2019).
- Zhu, G., Zhang, F., Ni, Q., Niu, G. & Chen, X. Efficient nanovaccine delivery in cancer immunotherapy. *ACS Nano* **11**, 2387–2392 (2017).
- Rezaei, M., Hosseini, S. N., Khavari-Nejad, R. A., Najafi, F. & Mahdavi, M. HBs antigen and mannose loading on the surface of iron oxide nanoparticles in order to immuno-targeting: fabrication, characterization, cellular and humoral immunoassay. *Artifi. Cells Nanomed. Biotechnol.* **47**, 1543–1558 (2019).
- Zhao, Y., Zhao, X., Cheng, Y., Guo, X. & Yuan, W. Iron oxide nanoparticles-based vaccine delivery for cancer treatment. *Mol. Pharm.* **15**, 1791–1799 (2018).
- Meng, J. et al. Two-pronged intracellular co-delivery of antigen and adjuvant for synergistic cancer immunotherapy. *Adv. Mater.* **34**, 2202168 (2022).
- Chyu, K.-Y. et al. Immunization using ApoB-100 peptide-linked nanoparticles reduces atherosclerosis. *JCI Insight* **7**, e149741 (2022).
- Yi, X. et al. Retinoic acid-loaded poly(lactic-co-glycolic acid) nanoparticle formulation of ApoB-100-derived peptide 210 attenuates atherosclerosis. *J. Biomed. Nanotechnol.* **16**, 467–480 (2020).
- Dimayuga, P. C. et al. Identification of apoB-100 peptide-specific CD8⁺ T cells in atherosclerosis. *J. Am. Heart Assoc.* **6**, e005318 (2017).
- Radovic-Moreno, A. F. et al. Immunomodulatory spherical nucleic acids. *Proc. Natl Acad. Sci. USA* **112**, 3892 (2015).
- Krieg, A. M. & Vollmer, J. Toll-like receptors 7, 8, and 9: linking innate immunity to autoimmunity. *Immunol. Rev.* **220**, 251–269 (2007).
- Hemmi, H. et al. A Toll-like receptor recognizes bacterial DNA. *Nature* **408**, 740–745 (2000).
- Liu, S. et al. A DNA nanodevice-based vaccine for cancer immunotherapy. *Nat. Mater.* **20**, 421–430 (2021).
- Yu, W. et al. Enhanced immunostimulatory activity of a cytosine-phosphate-guanosine immunomodulator by the assembly of polymer DNA wires and spheres. *ACS Appl. Mater. Interfaces* **12**, 17167–17176 (2020).
- Tan, X., Jia, F., Wang, P. & Zhang, K. Nucleic acid-based drug delivery strategies. *J. Control. Release* **323**, 240–252 (2020).
- Bachmann, M. F. & Jennings, G. T. Vaccine delivery: a matter of size, geometry, kinetics and molecular patterns. *Nat. Rev. Immunol.* **10**, 787–796 (2010).
- Molino, N. M., Anderson, A. K. L., Nelson, E. L. & Wang, S.-W. Biomimetic protein nanoparticles facilitate enhanced dendritic cell activation and cross-presentation. *ACS Nano* **7**, 9743–9752 (2013).
- Zhang, L. et al. Promoting the delivery of nanoparticles to atherosclerotic plaques by DNA coating. *ACS Appl. Mater. Interfaces* **11**, 13888–13904 (2019).
- Warren, T. L. et al. APC stimulated by CpG oligodeoxynucleotide enhance activation of MHC class I-restricted T cells. *J. Immunol.* **165**, 6244 (2000).
- Burgdorf, S., Kautz, A., Böhnert, V., Knolle, P. A. & Kurts, C. Distinct pathways of antigen uptake and intracellular routing in CD4 and CD8 T cell activation. *Science* **316**, 612–616 (2007).
- Jia, Q. et al. Gelification: an effective measure for achieving differently sized biocompatible Fe₃O₄ nanocrystals through a single preparation recipe. *J. Am. Chem. Soc.* **133**, 19512–19523 (2011).
- Dunlop, D. J. Superparamagnetic and single-domain threshold sizes in magnetite. *J. Geophys. Res.* **78**, 1780 (1973).
- Mahmoudi, M., Simchi, A., Milani, A. S. & Stroeve, P. Cell toxicity of superparamagnetic iron oxide nanoparticles. *J. Colloid Interface Sci.* **336**, 510–518 (2009).
- Choi, C. H. J., Hao, L., Narayan, S. P., Auyeung, E. & Mirkin, C. A. Mechanism for the endocytosis of spherical nucleic acid nanoparticle conjugates. *Proc. Natl Acad. Sci. USA* **110**, 7625–7630 (2013).

38. Pei, J. et al. Targeting lysosomal degradation pathways: new strategies and techniques for drug discovery. *J. Med. Chem.* **64**, 3493–3507 (2021).
39. Aderem, A. & Underhill, D. M. Mechanisms of phagocytosis in macrophages. *Annu. Rev. Immunol.* **17**, 593–623 (1999).
40. Schuette, V. et al. Mannose receptor induces T-cell tolerance via inhibition of CD45 and up-regulation of CTLA-4. *Proc. Natl Acad. Sci. USA* **113**, 10649–10654 (2016).
41. Wu, X. A., Choi, C. H., Zhang, C., Hao, L. & Mirkin, C. A. Intracellular fate of spherical nucleic acid nanoparticle conjugates. *J. Am. Chem. Soc.* **136**, 7726–7733 (2014).
42. van der Zande, H. J. P., Nitsche, D., Schlautmann, L., Guigas, B. & Burgdorf, S. The mannose receptor: From endocytic receptor and biomarker to regulator of (meta)inflammation. *Front. Immunol.* **12**, 765034 (2021).
43. Embgenbroich, M. & Burgdorf, S. Current concepts of antigen cross-presentation. *Front. Immunol.* **9**, 1643 (2018).
44. Musielak, M., Piotrowski, I. & Suchorska, W. M. Superparamagnetic iron oxide nanoparticles (SPIONs) as a multifunctional tool in various cancer therapies. *Rep. Pract. Oncol. Radiother.* **24**, 307–314 (2019).
45. Behzadi, M., Vakili, B., Ebrahiminezhad, A. & Nezafat, N. Iron nanoparticles as novel vaccine adjuvants. *Eur. J. Pharm. Sci.* **159**, 105718 (2021).
46. Okada, H. et al. Induction of CD8⁺ T-cell responses against novel glioma-associated antigen peptides and clinical activity by vaccinations with α -type 1 polarized dendritic cells and polyinosinic-polycytidylic acid stabilized by lysine and carboxymethylcellulose in patients with recurrent malignant glioma. *J. Clin. Oncol.* **29**, 330–336 (2010).
47. Sckisel, G. D. et al. Differential phenotypes of memory CD4 and CD8 T cells in the spleen and peripheral tissues following immunostimulatory therapy. *J. Immunother. Cancer* **5**, 33 (2017).
48. Lan X., Zebley C. C., Youngblood B. Cellular and molecular waypoints along the path of T cell exhaustion. *Sci. Immunol.* **8**, eadg3868 (2023).
49. Tietze, J. K. et al. Delineation of antigen-specific and antigen-nonspecific CD8⁺ memory T-cell responses after cytokine-based cancer immunotherapy. *Blood* **119**, 3073–3083 (2012).
50. Getz, G. S. & Reardon, C. A. Diet and murine atherosclerosis. *Arterioscler. Thromb. Vasc. Biol.* **26**, 242–249 (2006).
51. Reikhter, M. D. Collagen synthesis in atherosclerosis: too much and not enough. *Cardiovasc. Res.* **41**, 376–384 (1999).
52. Gisterå, A. et al. Low-density lipoprotein-reactive T cells regulate plasma cholesterol levels and development of atherosclerosis in humanized hypercholesterolemic mice. *Circulation* **138**, 2513–2526 (2018).
53. Shah, P. K., Chyu, K.-Y., Dimayuga, P. C. & Nilsson, J. Vaccine for atherosclerosis. *J. Am. Coll. Cardiol.* **64**, 2779–2791 (2014).
54. Chyu, K.-Y., Dimayuga, P. C. & Shah, P. K. Vaccine against arteriosclerosis: an update. *Ther. Adv. Vaccines* **5**, 39–47 (2017).
55. Zeng, Z. et al. Apolipoprotein B-100 peptide 210 antibody inhibits atherosclerosis by regulation of macrophages that phagocytize oxidized lipid. *Am. J. Transl. Res.* **10**, 1817–1828 (2018).
56. Dunér, P. et al. Antibodies against apoB100 peptide 210 inhibit atherosclerosis in apoE^{-/-} mice. *Sci. Rep.* **11**, 9022 (2021).
57. Kobiyama, K. et al. A clinically applicable adjuvant for an atherosclerosis vaccine in mice. *Eur. J. Immunol.* **48**, 1580–1587 (2018).
58. Zhou, J. et al. CD8⁺CD25⁺ T cells reduce atherosclerosis in apoE^{-/-} mice. *Biochem. Biophys. Res. Commun.* **443**, 864–870 (2014).
59. Noble, A., Giorgini, A. & Leggat, J. A. Cytokine-induced IL-10-secreting CD8 T cells represent a phenotypically distinct suppressor T-cell lineage. *Blood* **107**, 4475–4483 (2006).
60. Rohrer, J. W. & Cogglin, J. H. Jr. CD8 T cell clones inhibit antitumor T cell function by secreting IL-10. *J. Immunol.* **155**, 5719–5727 (1995).
61. Centa, M. et al. Acute loss of apolipoprotein E triggers an auto-immune response that accelerates atherosclerosis. *Arterioscler. Thromb. Vasc. Biol.* **38**, e145–e158 (2018).
62. Wolf, D. & Ley, K. Immunity and inflammation in atherosclerosis. *Circ. Res.* **124**, 315–327 (2019).
63. Jonasson, L., Holm, J., Skalli, O., Bondjers, G. & Hansson, G. K. Regional accumulations of T cells, macrophages, and smooth muscle cells in the human atherosclerotic plaque. *Arteriosclerosis* **6**, 131–138 (1986).
64. Koltsova, E. K. et al. Dynamic T cell-APC interactions sustain chronic inflammation in atherosclerosis. *J. Clin. Invest.* **122**, 3114–3126 (2012).
65. Herbin, O. et al. Regulatory T-cell response to apolipoprotein B100-derived peptides reduces the development and progression of atherosclerosis in mice. *Arterioscler. Thromb. Vasc. Biol.* **32**, 605–612 (2012).
66. Nettersheim, F. S., De Vore, L. & Winkels, H. Vaccination in atherosclerosis. *Cells* **9**, 2560 (2020).
67. Berg, R. E. & Forman, J. The role of CD8 T cells in innate immunity and in antigen non-specific protection. *Curr. Opin. Immunol.* **18**, 338–343 (2006).
68. Saigusa, R., Winkels, H. & Ley, K. T cell subsets and functions in atherosclerosis. *Nat. Rev. Cardiol.* **17**, 387–401 (2020).
69. Flores, R. R., Diggs, K. A., Tait, L. M. & Morel, P. A. IFN- γ negatively regulates CpG-induced IL-10 in bone marrow-derived dendritic cells. *J. Immunol.* **178**, 211–218 (2007).
70. Hu, X. et al. IFN- γ suppresses IL-10 production and synergizes with TLR2 by regulating GSK3 and CREB/AP-1 proteins. *Immunity* **24**, 563–574 (2006).
71. Imbrechts, M. et al. IFN- γ stimulates CpG-induced IL-10 production in B cells via p38 and JNK signalling pathways. *Eur. J. Immunol.* **48**, 1506–1521 (2018).
72. Li, X.-Q., Meng, F.-T., Ma, G.-H. & Su, Z.-G. A simple and efficient method for synthesis of carboxymethylated polyethyleneglycol. *J. Chem. Res.* **2005**, 280–281 (2005).
73. Lutz, M. B. et al. An advanced culture method for generating large quantities of highly pure dendritic cells from mouse bone marrow. *J. Immunol. Methods* **223**, 77–92 (1999).

Acknowledgements

We thank the financial support from the National Natural Science Foundation of China 81801839 (L. Zhang), 82200497 (H. Zhang), 21904069 (W. Zhu), 22274079 (W. Zhu), 51873087 (C. Chen) and 51803092 (D. Sun), and the Natural Science Foundation of Jiangsu Province BK20190653 (W. Zhu) and BK20240131 (W. Zhu). We thank Dr. Xin Wang from Jiangsu Cancer Hospital for his help with flow cytometric design and analysis, and consultation. We thank Dr. Shanyue Guan from Technical Institute of Physics and Chemistry, CAS for her help with nanoparticle characterizations. We thank Prof. Huaping Tan from the School of Materials Science and Engineering at Nanjing University of Science and Technology (NJUST) for cryostat sectioning. We thank Ms. Lanlan Zhang from School of Electronic and Optical Engineering, NJUST for her help with the confocal imaging. We thank Dr. Long Ma, Mr. Tao Zheng, and Ms. Qingqing Zhou from Nanjing Jinling Hospital for their help with in vivo fluorescence imaging.

Author contributions

L. Zhang, C. Chen, H. Zhang, W. Zhu, and D. Sun provided the funding. L. Zhang and A. AL-Ammari conceived the idea, designed the experiments, performed most of the in vitro and in vivo experiments, and analyzed the data. P. Zhou performed part of the in vitro experiments. W. Ding, X. Li, Q. Yu, and Y. Gai performed some in vivo experiments and analyzed the data. D. Zhu and X. Ma performed the flow cytometric

analysis and helped with analyzing flow cytometry data. C. Zuo and L. Zhang performed the confocal imaging and analyzing data. H. Zhang and W. Zhu contributed to the design of animal experiments. L. Zhang, A. AL-Ammari, P. Zhou, and X. Zhi drafted the manuscript. H. Zhang, J. Zhang, and W. Zhu revised the paper.

Competing interests

The authors declare no competing interest.

Additional information

Supplementary information The online version contains supplementary material available at <https://doi.org/10.1038/s41467-025-57467-5>.

Correspondence and requests for materials should be addressed to Jiaan Zhang, Wanying Zhu or Dongping Sun.

Peer review information *Nature Communications* thanks Xiaoyuan Chen and the other anonymous reviewer(s) for their contribution to the peer review of this work. A peer review file is available.

Reprints and permissions information is available at <http://www.nature.com/reprints>

Publisher's note Springer Nature remains neutral with regard to jurisdictional claims in published maps and institutional affiliations.

Open Access This article is licensed under a Creative Commons Attribution-NonCommercial-NoDerivatives 4.0 International License, which permits any non-commercial use, sharing, distribution and reproduction in any medium or format, as long as you give appropriate credit to the original author(s) and the source, provide a link to the Creative Commons licence, and indicate if you modified the licensed material. You do not have permission under this licence to share adapted material derived from this article or parts of it. The images or other third party material in this article are included in the article's Creative Commons licence, unless indicated otherwise in a credit line to the material. If material is not included in the article's Creative Commons licence and your intended use is not permitted by statutory regulation or exceeds the permitted use, you will need to obtain permission directly from the copyright holder. To view a copy of this licence, visit <http://creativecommons.org/licenses/by-nc-nd/4.0/>.

© The Author(s) 2025